Dynamic Modelling of MacPherson and double wishbone suspension

A Project Report

submitted by

SUNNY BHATI
ED10B042

in partial fulfilment of the requirements
for the award of the degree of

MASTER OF TECHNOLOGY in AUTOMOTIVE ENGINEERING
AND
BACHELOR OF TECHNOLOGY in ENGINEERING DESIGN

DEPARTMENT OF ENGINEERING DESIGN
INDIAN INSTITUTE OF TECHNOLOGY MADRAS

June 2015

REPORT CERTIFICATE

This is to certify that the report titled **Dynamic modelling of MacPherson and double wishbone suspension**, submitted by **Sunny Bhati**, to the Indian Institute of Technology, Madras, for the award of the degree of **Master of Technology**, is a bona fide record of the research work done by him under the supervision of Dr. Sandipan Bandyopadhyay. The contents of this report, in full or in parts, have not been submitted to any other Institute or University for the award of any degree or diploma.

Prof. Sandipan Bandyopadhyay
Research Guide
Assistant Professor
Department of Engineering Design
IIT-Madras
Chennai,600 036

Prof. Srikanth Vedantam
Head of department (In-charge)
Professor
Department of Engineering Design
IIT-Madras
Chennai, 600 036

Place: Chennai

Date: 13th June 2015

ACKNOWLEDGEMENTS

I would like to convey my gratitude towards my guide Dr. Sandipan Bandyopadhyay for his invaluable contribution towards the inception of the idea in my mind. I am deeply indebted towards him for his constant support throughout the project.

I would also like to express gratitude towards Ram, Rishika, Sushant, and my wingmates, people who personify the true meaning of friendship, in maintaining a cheerful work atmosphere and for motivating me throughout my project.

Most importantly, I am thankful to my parents who have given me strength and placed a major role in shaping me into the person who I am. The confidence that they show in me, has always motivated me to make the right choice to the best of my knowledge.

ABSTRACT

KEYWORDS: Lagrangian dynamics; MacPherson suspension; double wishbone; actuator space; configuration space

Suspension and steering system is one of the most important assemblies in a car. Its design is a very complex, time-consuming and important part of the vehicle design process. It has to perform effectively under a wide range and combinations of operating conditions including high levels of braking and acceleration, cornering at high speeds and traversing rough terrains. Double wishbone suspension and MacPherson suspension are two of the most popular suspensions in use today.

The objective of this work is to use an existing kinematic model of the MacPherson and the double wishbone suspension to formulate the dynamics of the suspensions using Lagrangian method in actuator and configuration space. In the first part, Lagrangian formulation for closed-loop mechanisms has been presented in detail, along with the verifications that are necessary to validate the correctness of the formulation.

In the second part, a spatial kinematic model of double wishbone and MacPherson from [1] is presented in detail, which is used in the formulation of loop-closure equations so as to formulate the equation of motion for the suspension system. The formulation of the suspension dynamics in actuator and configuration space has been done in two ways, i.e., firstly, considering the suspension as a mass spring model, and secondly, considering the suspension as mass spring damper system. Results validating the formulation of the MacPherson strut and double wishbone suspension in configuration and actuator spaces have been presented in detail. Equation of motion of these system are in the form of differential equations. Therefore, solving differential equations with less computational time is very important. In the next part, various methods to solve differential equations formed in actuator space and configuration space have been presented along with their computational time. Finally, a comparative study indicating which formulation is computationally more feasible with regard to the computational ease has been presented.

TABLE OF CONTENTS

LIST OF TABLES

LIST OF FIGURES

ABBREVIATIONS

DWB	Double wishbone
MPS	MacPherson Strut

CHAPTER 1

INTRODUCTION

Suspension system in an automobile plays a crucial role in reducing the mutual influence between wheels and improving dynamic behaviour. In reality, it has to perform effectively under a wide range and combinations of operating conditions. For this, vertical compliance is necessary to provide chassis isolation and to ensure wheels follow the road profile. Steering control during cornering is another equally important requirement, which needs the wheels to be maintained at a certain position and orientation. Other requirements being isolating the vehicle from high frequency vibration arising from tyre excitation and to control forces and torques at tyre road interface.

Suspension systems can be classified as dependent or independent depending on their topology and how they are connected to wheels. Different topologies exist in independent suspension design, such as double wishbone suspension, MacPherson suspension, trailing arm, swing axles and multi-link suspensions. From kinematics point of view, suspension system design is a combination of links and joints, while dynamically, a good suspension should be able to isolate the vibrations experienced at the road tyre.

Computational tools exist today such as ADAMS, CAD to conceptualize the ideas and simulate the design under various operating conditions. Modelling the dynamics of DWB and MPS suspension involves various elements and is often, a very complex and time consuming process. Therefore, it is essential to build a computational framework where we can study the dynamics of DWB and MPS suspension systems. As a mechanism, both DWB and MPS possess two $degree-of-freedom$: one accounting for the steering input *s(t)*, and the other accommodating bounce and rebound, the road profile input *y(t)*.

The dynamical formulation has been implemented on the kinematic model as proposed in Madhu Kodati et al (2015). Two different formulations has been presented, one in configuration space and other in actuator space for both MPS and DWB suspension system and consequently, results have been verified.

Computational time is an important aspect while formulating the mechanism, as it is an indicator of the complexity of the mechanism. Computational time has been presented and studied in this report while constructing the method in the configuration space as well as actuator space.

1.1 Double wishbone suspension

The DWB, shown in the Fig. 1.1 is the most common front suspension of the American cars following World War 2. It is also known as double A-arm and short-long arm suspension.

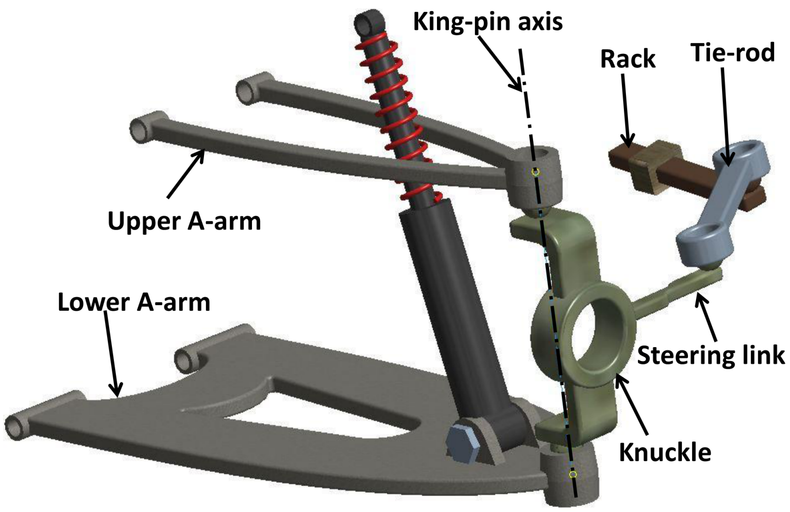

Figure 1.1: Simplified solid model of double wishbone suspension (taken from [1]).

Each wishbone or arm has two mounting points to the chassis and connected to the knuckle by a spherical joint. The damper and coil spring system is placed between chassis and either of the control arms to control vertical movement.

In case of front axle suspension, the steering link is attached to the tie-rod using spherical joints, and the tie-rod is connected to the rack with a universal joint. The DWB is used in high-performance vehicles and SUVs due to its superior kinematic response [2].

1.2 MacPherson strut suspension

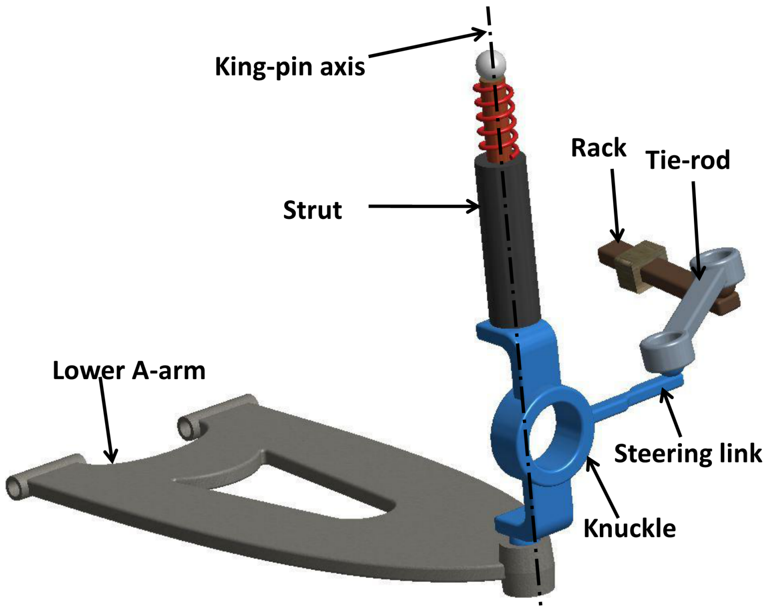

Figure 1.2: Simplified solid model of MacPherson strut (taken from [1]).

American automotive engineer Earle S. MacPherson developed the MPS using a strut configuration. As shown in Fig. 1.2 one end of the strut is attached to the knuckle with prismatic joint and other end is fixed to the chassis by spherical joint. The strut also contains the spring and damping elements. The lower arm is fixed to chassis by revolute joint and other end is connected to knuckle by spherical joint. The steering link is attached to the tie-rod using spherical joints and tie-rod is connected to rack with a universal joint. The MPS provides major advantages in package space for transverse engines and thus is used widely for front wheel drive cars.

1.3 Objectives

The objective of the report is to formulate the dynamics of the suspension using Lagrangian formulation in actuator and configuration space and understand the computational advantages or disadvantages associated with the formulations. The simulation performed has no physical significance as s and y are step inputs, which is not observed in real time environment. The effect of vehicle dynamics has not been included in the formulation. Arbitrary value of s and y has been taken to validate the correctness of the formulation.

Based on the motivation, the problem is divided into the following parts:

1. To develop the equation of the motion of the DWS and MPS in the configuration space.
2. To develop the equation of motion of the DWS and MPS in the actuator space.
3. To verify the correctness of the model with zeroth order check, first order check and energy check, which will be described in Chapter 2.
4. To analyze and perform a comparative analysis on the computational time taken to solve the MPS and DWB in configuration and actuator space.

1.4 Modelling assumptions

The report while studying the dynamics of the DWS and MPS deals with the following assumptions:

1. The cushioning effect of the bushes at the joints are not considered, i.e., only ideal joints are considered in the formulation.
2. The flexibility of the links are not considered, only rigid links are used in the formulation.
3. The chassis is considered to be fixed or the ground link in the mechanism.
4. All the geometric parameters of the suspension are exactly known.
5. The universal joint between the tie rod and the rack is replaced with a spherical joint.

1.5 Organization of the report

The report has been organized into five chapters, the Chapter 1 deals with the introduction of the suspension and different types of suspensions used in automotive industry.

The Chapter 2 deals with background on kinematics and dynamics of closed-loop mechanisms in configuration and actuator space using Lagrangian formulation.

The Chapter 3 deals specifically with kinematics and dynamic formulation of MacPherson strut suspension in configuration and actuator space using Lagrangian formulation and results have been presented along with the validation plots to check the correctness of the formulation.

The Chapter 4 deals with kinematics and dynamic formulation of double wishbone suspension in configuration and actuator space using Lagrangian formulation and results have been presented along with the validation plots to check the accuracy of the formulation. Finally, the conclusions and the future work is proposed in Chapter 5.

CHAPTER 2

DYNAMICS OF CLOSED-LOOP MECHANISMS

2.1 Introduction

Generally, there are three types of mechanisms, namely, serial mechanism, parallel mechanism and mixed or hybrid mechanism (i.e., combination of both serial and parallel). Serial mechanism have a single kinematic chain with actuators, connecting the base to end-effector. On the other hand, parallel with $n\ degree - of - freedom$ has two or more kinematic chains which connect the base to end-effector. The suspension system MPS and DWB, both belongs to the class of parallel mechanism. Both the mechanisms possess two $degree - of - freedom$: one arising because of the steering input *s(t)* and the other due to the road profile input *y(t)*. In order to study any mechanism completely, we need to understand the kinematics and dynamics of it, which allows us to study the aspects like singularities, velocity and acceleration capabilities. This chapter includes the detailed study of the formulation of the dynamics equation using Lagrangian in configuration space and in the later part, a systematic method to formulate the dynamics in actuator space has been presented.

2.2 Kinematics

Kinematics of a mechanism gives the position, velocity and higher derivatives of the position variables with respect to time or other variables. It also gives us the information about the kinematic branches of the mechanism.

In $n\ degree{-}of{-}freedom$ mechanism, the configuration at an instant can be represented using two sets of variables. The first set of link variables $\boldsymbol{\theta} = [\theta_1, \ldots, \theta_n]^\top$, associated with the links which are actuated by actuators like prismatic and rotary, are termed as active variables. The second set of links are governed indirectly by loop closure equations and therefore, the link variables $\boldsymbol{\phi} = [\phi_1, \ldots, \phi_m]^\top$ are termed as passive variables. The configuration of the mechanism is represented using $\boldsymbol{\theta}$ and $\boldsymbol{\phi}$, therefore the variable $\boldsymbol{q} = [\boldsymbol{\theta}^\top, \boldsymbol{\phi}^\top]^\top$ is termed as configuration variable. For example, the variables for a four bar mechanism are represented in Fig. 2.1, where $\boldsymbol{\theta} = \theta_1$ and , $\boldsymbol{\phi} = [\phi_2, \phi_3]^\top$. The set of variables $\boldsymbol{x} = [x, y]^\top$ are termed as task space variables (i.e., the space which represents the motion of end- effector).

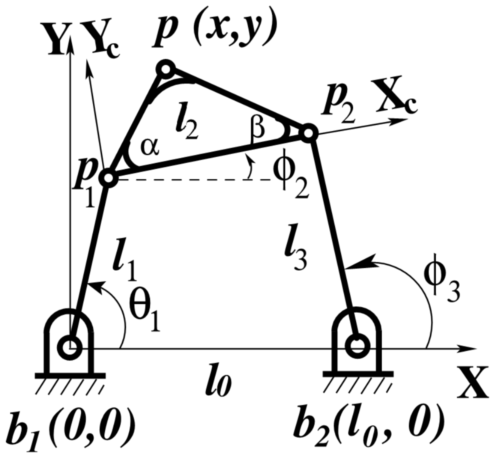

Figure 2.1: Kinematic model of a four-bar mechanism.

The zeroth order kinematics involves forward and inverse kinematics, which is to find $\boldsymbol{\phi}$ for a given value of $\boldsymbol{\theta}$, and to find the $\boldsymbol{\theta}$ for a given value of $\boldsymbol{x}$, respectively.

For zeroth order kinematics the relation between variables are given by loop closure equations $\boldsymbol{\eta}(\boldsymbol{q}) = \mathbf{0}$. For example, the loop closure equation for four-bar mechanism can be written as:

$$\boldsymbol{\eta}(\boldsymbol{\theta}, \boldsymbol{\phi}) = \begin{bmatrix} l_1 \cos\theta_1 + l_2 \cos\phi_2 - l_0 - l_3 \cos\phi_3 \\ l_1 \sin\theta_1 + l_2 \sin\phi_2 - l_3 \sin\phi_3 \end{bmatrix}, \tag{2.1}$$

where, $\boldsymbol{\eta} \in \mathbb{R}^m$ ($m = 2$ for four-bar mechanism) where m is the number of constraints that is equal to the number of passive variables. Similarly, first and second order kinematics deals with the velocity and acceleration of any point on the mechanism.

2.3 Dynamics

The formulation of the equation of motion for mechanism is done using two common methods, namely, the Newton-Euler and Lagrangian method. Often, Lagrangian method is preferred as it produces the equation of motion in a structured manner, which is quite helpful in further analysis and can be implemented symbolically. Equation of motion in configuration space is formulated using the constrained Lagrangian formulation [3]. The general equation of motion for constrained rigid- body system can be written as,

$$\boldsymbol{M}\ddot{\boldsymbol{q}} + \boldsymbol{C}\dot{\boldsymbol{q}} + \boldsymbol{G} = \boldsymbol{\tau} + \boldsymbol{J}_{\eta q}^{\top}\boldsymbol{\lambda}, \tag{2.2}$$

where, $\boldsymbol{\lambda}$ is a vector of unidentified multipliers, $\boldsymbol{J}_{\eta q}^{\top}\boldsymbol{\lambda}$ term represents constraint forces or moments, associated with the constraints. The method to compute $\boldsymbol{M}$, $\boldsymbol{C}$, $\boldsymbol{G}$ and to convert constrained Lagrangian equation of motion into actuator space is presented in this section.

2.3.1 Method to compute $\boldsymbol{M}$, $\boldsymbol{C}$, and $\boldsymbol{G}$ matrices

The terms $\boldsymbol{M}, \boldsymbol{C},$ and $\boldsymbol{G}$ are obtained using the Euler-Lagrangian formulation. The general equations of motion for a closed-loop mechanism is given in Eq. (2.1). The method to compute them is given in this section.

Mass matrix ($\boldsymbol{M}$)

Derivation of the motion of a single rigid body can be conceptually decomposed to a translation of the center of mass and a rotation about the center. Let us denote the velocity of translation by $\boldsymbol{v}_i$ and the angular velocity of rotation by $\boldsymbol{\omega}_i$ for the ith body of the mechanism. Then kinetic energy of the ith body of the mechanism is given by,

$$T_i = \frac{1}{2} m_i \boldsymbol{v}_i^{\top} \boldsymbol{v}_i + \frac{1}{2} \boldsymbol{\omega}_i^{\top} \boldsymbol{I}_i \boldsymbol{\omega}_i, \tag{2.3}$$

where, m_i is the mass and $\boldsymbol{I}_i$ is the inertia tensor w.r.t center of mass. The translational velocity and rotational velocity can be represented in terms of configuration space coordinates, $\boldsymbol{q}$, and as a linear combination of time-derivatives $\dot{\boldsymbol{q}}$,

$$\boldsymbol{v}_i = \boldsymbol{J}_{\boldsymbol{v}_i}\dot{\boldsymbol{q}}, \tag{2.4}$$

$$\boldsymbol{\omega}_i = \boldsymbol{J}_{\boldsymbol{\omega}_i}\dot{\boldsymbol{q}}. \tag{2.5}$$

Substituting Eq. (2.4) and Eq. (2.5), in Eq. (2.3), the total kinetic energy of the mechanism with k number of links is given by,

$$T = \frac{1}{2}\dot{\boldsymbol{q}}^\top \boldsymbol{M}\dot{\boldsymbol{q}}, \text{ where,} \tag{2.6}$$
$$\boldsymbol{M} = \sum_{i=1}^{k}(m_i \boldsymbol{J}_{\boldsymbol{v}_i}^\top \boldsymbol{J}_{\boldsymbol{v}_i} + \boldsymbol{J}_{\boldsymbol{\omega}_i}^\top \boldsymbol{I}_i \boldsymbol{J}_{\boldsymbol{\omega}_i}).$$

It is to noted that matrix $\boldsymbol{M}$ can be treated as the effective mass/inertia (matrix) of the manipulator. $\boldsymbol{M}$ is symmetric and positive-definite matrix.

Centripetal and Coriolis matrix ($\boldsymbol{C}$)

The centripetal and Coriolis matrix $\boldsymbol{C}$ is computed from the $\boldsymbol{M}$ matrix as follows:

$$\boldsymbol{C}_{ij} = \frac{1}{2}\sum_{k=1}^{n}\left(\frac{\partial \boldsymbol{M}_{ij}}{\partial \boldsymbol{q}_k} + \frac{\partial \boldsymbol{M}_{ik}}{\partial \boldsymbol{q}_j} - \frac{\partial \boldsymbol{M}_{kj}}{\partial \boldsymbol{q}_i}\right)\dot{\boldsymbol{q}}_k. \tag{2.7}$$

It can be noted that the $\boldsymbol{C}$ matrix depends on both $\boldsymbol{q}$ and $\dot{\boldsymbol{q}}$.

Gravity term ($\boldsymbol{G}$)

The gravity term $\boldsymbol{G}$ is a vector quantity, it is computed by taking the partial derivative of the total potential energy of the system with respect to configuration variables:

$$\boldsymbol{G} = \frac{\partial V}{\partial \boldsymbol{q}}, \tag{2.8}$$

where, V is the total potential energy of the system.

2.3.2 Actuator space formulation

The equations of motion for the mechanism in actuator space $\boldsymbol{\theta}$ can be obtained from Eq. (2.2) by eliminating $\boldsymbol{\lambda}$. We can rewrite Eq. (2.2) as:

$$\boldsymbol{M}\ddot{\boldsymbol{q}} + \boldsymbol{C}\dot{\boldsymbol{q}} + \boldsymbol{G} - \boldsymbol{\tau} - \boldsymbol{J}_{\eta q}^{\top}\boldsymbol{\lambda} = \mathbf{0}. \tag{2.9}$$

Pre-multiplying Eq. (2.9) by $\dot{\boldsymbol{q}}^{\top}$, we get:

$$\dot{\boldsymbol{q}}^{\top}\boldsymbol{M}\ddot{\boldsymbol{q}} + \dot{\boldsymbol{q}}^{\top}\boldsymbol{C}\dot{\boldsymbol{q}} + \dot{\boldsymbol{q}}^{\top}\boldsymbol{G} - \dot{\boldsymbol{q}}^{\top}\boldsymbol{\tau} - \dot{\boldsymbol{q}}^{\top}\boldsymbol{J_{\eta q}}^{\top}\boldsymbol{\lambda} = 0. \tag{2.10}$$

Taking first derivative of $\boldsymbol{\eta}(\boldsymbol{q}) = \mathbf{0}$ w.r.t. time, we can write:

$$\dot{\boldsymbol{q}}^{\top}\boldsymbol{J_{\eta q}}^{\top} = \mathbf{0}. \tag{2.11}$$

Rewriting Eq. (2.11), we get:

$$\begin{aligned}
&\boldsymbol{J_{\eta\theta}}\dot{\boldsymbol{\theta}} + \boldsymbol{J_{\eta\phi}}\dot{\boldsymbol{\phi}} = \mathbf{0},\\
&\dot{\boldsymbol{\phi}} = -\boldsymbol{J_{\eta\phi}}^{-1}\boldsymbol{J_{\eta\theta}}\dot{\boldsymbol{\theta}} = \boldsymbol{J_{\phi\theta}}\dot{\boldsymbol{\theta}}, \ \text{ where, } \boldsymbol{J_{\phi\theta}} = -\boldsymbol{J_{\eta\phi}}^{-1}\boldsymbol{J_{\eta\theta}}
\end{aligned} \tag{2.12}$$

Using Eq. (2.12), we can write $\dot{\boldsymbol{q}}$ in terms of $\dot{\boldsymbol{\theta}}$ as:

$$\dot{\boldsymbol{q}} = \begin{bmatrix} \dot{\boldsymbol{\theta}} \\ \dot{\boldsymbol{\phi}} \end{bmatrix} = \begin{bmatrix} \boldsymbol{I}_n \\ \boldsymbol{J}_{\phi\theta} \end{bmatrix} \dot{\boldsymbol{\theta}} = \boldsymbol{J}_{q\theta}\dot{\boldsymbol{\theta}}, \tag{2.13}$$

where $\boldsymbol{I}_n$ is an identity matrix of order $n \times n$. Differentiating Eq. (2.13) w.r.t. time, we get:

$$\ddot{\boldsymbol{q}} = \boldsymbol{J}_{q\theta}\ddot{\boldsymbol{\theta}} + \dot{\boldsymbol{J}}_{q\theta}\dot{\boldsymbol{\theta}}. \tag{2.14}$$

Therefore, in Eq. (2.10), $\dot{\boldsymbol{q}}^{\top}\boldsymbol{J}_{\eta q}^{\top}\boldsymbol{\lambda} = 0$ for any $\boldsymbol{\lambda}$. This eliminates the constraint force term, and creates the equivalent unconstrained dynamical system as:

$$\dot{\boldsymbol{q}}^{\top}\boldsymbol{M}\ddot{\boldsymbol{q}} + \dot{\boldsymbol{q}}^{\top}\boldsymbol{C}\dot{\boldsymbol{q}} + \dot{\boldsymbol{q}}^{\top}\boldsymbol{G} - \dot{\boldsymbol{q}}^{\top}\boldsymbol{\tau} = 0. \tag{2.15}$$

Substituting $\dot{\boldsymbol{q}}, \ddot{\boldsymbol{q}}$ from Eqs. (2.13)and (2.14) into Eq. (2.15), we get:

$$\dot{\boldsymbol{\theta}}^\top(\boldsymbol{J}_{q\theta}^\top \boldsymbol{M}\boldsymbol{J}_{q\theta}\ddot{\boldsymbol{\theta}} + \boldsymbol{J}_{q\theta}^\top(\boldsymbol{M}\dot{\boldsymbol{J}}_{q\theta} + \boldsymbol{C}\boldsymbol{J}_{q\theta})\dot{\boldsymbol{\theta}} + \boldsymbol{J}_{q\theta}^\top \boldsymbol{G} - \boldsymbol{J}_{q\theta}^\top \boldsymbol{\tau}) = 0. \tag{2.16}$$

Eq. (2.16) is satisfied for any arbitrary $\dot{\boldsymbol{\theta}}$ and therefore,

$$\boldsymbol{J}_{q\theta}^\top \boldsymbol{M}\boldsymbol{J}_{q\theta}\ddot{\boldsymbol{\theta}} + \boldsymbol{J}_{q\theta}^\top(\boldsymbol{M}\dot{\boldsymbol{J}}_{q\theta} + \boldsymbol{C}\boldsymbol{J}_{q\theta})\dot{\boldsymbol{\theta}} + \boldsymbol{J}_{q\theta}^\top \boldsymbol{G} - \boldsymbol{J}_{q\theta}^\top \boldsymbol{\tau} = \boldsymbol{0}. \tag{2.17}$$

Further, Eq. (2.17) can be compactly written as:

$$\boldsymbol{M}_{\boldsymbol{\theta}}\ddot{\boldsymbol{\theta}} + \boldsymbol{C}_{\boldsymbol{\theta}}\dot{\boldsymbol{\theta}} + \boldsymbol{G}_{\boldsymbol{\theta}} = \boldsymbol{\tau}_{\boldsymbol{\theta}}, \tag{2.18}$$

where, $\boldsymbol{M}_{\boldsymbol{\theta}} = \boldsymbol{J}_{q\theta}^\top \boldsymbol{M}\boldsymbol{J}_{q\theta},\ \boldsymbol{C}_{\boldsymbol{\theta}} = \boldsymbol{J}_{q\theta}^\top(\boldsymbol{M}\dot{\boldsymbol{J}}_{q\theta} + \boldsymbol{C}\boldsymbol{J}_{q\theta}),\ \boldsymbol{G}_{\boldsymbol{\theta}} = \boldsymbol{J}_{q\theta}^\top \boldsymbol{G},\ \boldsymbol{\tau}_{\boldsymbol{\theta}} = \boldsymbol{J}_{q\theta}^\top \boldsymbol{\tau}$.

2.4 Validation of the numerical results

Three checks are necessary to validate the formulation and check the correctness of the model.

1. **Zeroth order check:** This check is required to ensure that the constraint equation, $\|\boldsymbol{\eta}(\boldsymbol{q})\| < \epsilon$, ϵ being a small positive real number, is satisfied throughout the simulation time.

2. **First order check:** This check is required to ensure that $\|\boldsymbol{J}_{\eta q}\dot{\boldsymbol{q}}\| < \epsilon$ is satisfied throughout the simulation time.

3. **Energy check:** This check is necessary to check the correctness of the formulation. In the absence of non-conservative forces or torques acting on the system, the energy of the mechanism has to remain conserved. Therefore, for free fall simulation of the mechanism i.e. only gravity is acting, the energy of the system should be conserved.

2.5 Conclusion

In this chapter, the background on kinematics and formulation of dynamics in actuator space of the closed-loop mechanism has been presented. The verification checks to validate the correctness of the formulation of the mechanism has also been presented in detail.

CHAPTER 3

DYNAMIC FORMULATION OF MACPHERSON STRUT SUSPENSION

Spatial kinematic model of MacPherson suspension as presented in a work by Madhu Kodati [1] is used in the formulation of the equation of dynamics. Details of the kinematic model have been included in the first part of this chapter for the sake of completeness. Later, the formulation for the dynamics of the MacPherson suspension system has been presented with validations to check the correctness of the formulation.

3.1 Kinematic model

A comprehensive spatial kinematic model of MacPherson has been presented in this section.

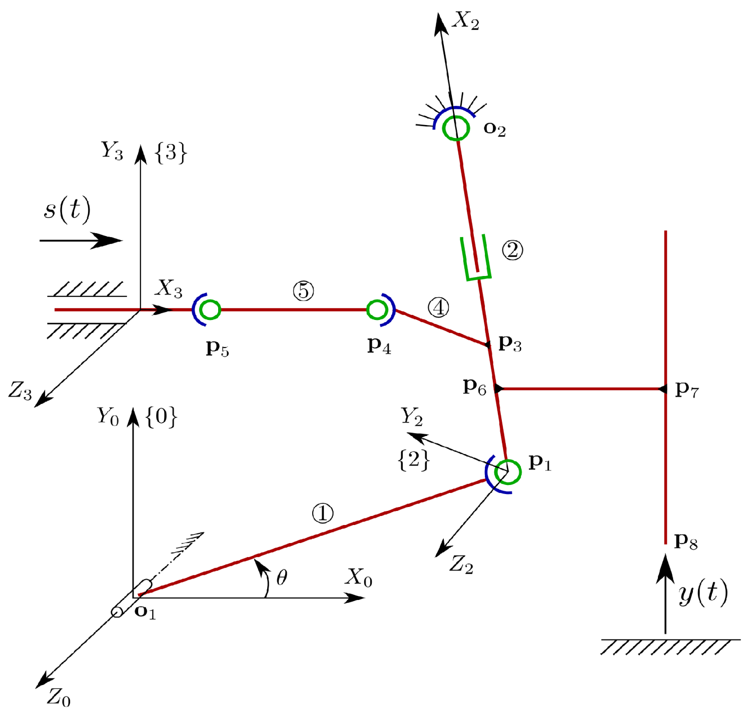

Figure 3.1: Kinematic model of MacPherson strut suspension (taken from [1]).

The schematic model of MPS suspension is as shown in Fig. 3.1. Kinematically, it is a combination of spatial four-bar mechanism $\boldsymbol{o}_1\boldsymbol{p}_1\boldsymbol{o}_2\boldsymbol{o}_1$, i.e., inverted slider mechanism a that has the chassis as the ground link, king-pin as the coupler and a spatial five-bar mechanism. These two mechanism are coupled at the king-pin.

Two co- ordinate systems are used to define the system. The global frame of reference $\{0\}$ is attached to $\boldsymbol{o}_1$, and its Z_0-axis is aligned to the axis of the hinges of the lower A- arm. Link 1 moves in the X_0Y_0 plane. The joint between $\boldsymbol{p}_1$ and $\boldsymbol{o}_2$ is considered to be a single prismatic joint of variable length l_2. A body frame of reference, $\{2\}$ is attached to $\boldsymbol{p}_1$. The X -axis of $\{2\}$ (denoted by X_2) is along the vector $\boldsymbol{l}_2 = \boldsymbol{o}_2 - \boldsymbol{p}_1$ and X_2Y_2 contains the link 4.

The rotation matrix ${}^0_3\mathbf{R}$ relating the orientation of frame $\{3\}$ to $\{0\}$ has been parameterized in terms of $XYZ\ Euler\ angles$, $(\beta_1,\ \beta_2, \beta_3)$(see [3]).

$$ {}^0_3\mathbf{R} = \mathbf{R}_X(\beta_1)\mathbf{R}_Y(\beta_2)\mathbf{R}_Z(\beta_3), \tag{3.1} $$

Simlarily, the rotation matrix ${}^0_2\mathbf{R}$ relating the orientation of frame $\{2\}$ to $\{0\}$ has been parameterized in terms of Rodrigue's parameters, $\boldsymbol{c} = [c_1, c_2, c_3]^\top \in R^{\,3}$(see [3]).

3.1.1 Formulation of the loop - closure equations

The loop closure equation as obtained in Eq. (A.14) can be represented as:

$$ \boldsymbol{\eta}_4 = \boldsymbol{p}_4 - \boldsymbol{p}_5 - {}^0_4\boldsymbol{R}[l_5, 0, 0]^\top = \mathbf{0}, \tag{3.2} $$

where, ${}^0_4\mathbf{R} = \mathbf{R}_Y(\beta)\mathbf{R}_Z(\gamma)$.

β and γ are the Euler-angle of the tie-rod about the Y-axis and Z-axis of the global reference frame $\{0\}$.

The Eq. (3.2) can be written as:

$$
\begin{aligned}
\boldsymbol{\eta}_4 =&[\eta_{4x},\ \eta_{4y}, \eta_{4z}]^\top, && (3.3)\\
\eta_{4x} =&- s\cos\beta_2\cos\beta_3 + \frac{r(1+c_1^2-c_2^2-c_3^2)}{1+c_1^2+c_2^2+c_3^2} + l_1\cos\theta - l_5\cos\beta\cos\gamma \\
&+ \frac{(1+c_1^2-c_2^2-c_3^2)l_{4x}}{1+c_1^2+c_2^2+c_3^2} + \frac{(2c_1c_2-2c_3)l_{4y}}{1+c_1^2+c_2^2+c_3^2} + \frac{2(c_2+c_1c_3)l_{4z}}{1+c_1^2+c_2^2+c_3^2} - p_{5x}, && (3.4)\\
\eta_{4y} =&- s(\cos\beta_3\sin\beta_1\sin\beta_2 + \cos\beta_1\sin\beta_3) + \frac{2r(c_1c_2+c_3)}{1+c_1^2+c_2^2+c_3^2} + l_1\sin\theta - l_5\sin\gamma \\
&+ \frac{2(c_1c_2+c_3)l_{4x}}{1+c_1^2+c_2^2+c_3^2} + \frac{(1-c_1^2+c_2^2-c_3^2)l_{4y}}{1+c_1^2+c_2^2+c_3^2} - \frac{2(c_1-c_2c_3)l_{4z}}{1+c_1^2+c_2^2+c_3^2} - p_{5y}, && (3.5)\\
\eta_{4z} =&- s(-\cos\beta_1\cos\beta_3\sin\beta_2 + \sin\beta_1\sin\beta_3) + \frac{2r(-c_2+c_1c_3)}{1+c_1^2+c_2^2+c_3^2} + l_5\cos\gamma\sin\beta \\
&+ \frac{2(-c_2+c_1c_3)l_{4x}}{1+c_1^2+c_2^2+c_3^2} + \frac{2(c_1+c_2c_3)l_{4y}}{1+c_1^2+c_2^2+c_3^2} + \frac{(1-c_1^2-c_2^2+c_3^2)l_{4z}}{1+c_1^2+c_2^2+c_3^2} - p_{5z}. && (3.6)
\end{aligned}
$$

Therefore, the constraint set of equations used in the formulation of dynamics can be expressed as:

$$\boldsymbol{\eta} = [\eta_{1x}, \eta_{1y}, \eta_{1z}, \eta_{3x}, \eta_{3y}, \eta_{3z}, \eta_{4x}, \eta_{4y}, \eta_{4z}]^\top.$$

The constraint equations $\eta_{1x}, \eta_{1y}, \eta_{1z}, \eta_{3x}, \eta_{3y}, \eta_{3z}$ are presented in detail in Section A.1 (taken from [1]).

Table 3.1: Geometric and mass values (taken from [5], with minor modifications).

Parameter	**Symbol**	**Value**
Length of lower-A arm	l_1	0.322
Length of tie rod	l_5	0.361
Link-4vector w.r.t.$\{2\}$	(l_{4x}, l_{4y}, l_{4z})	(0,0.108,0)
Position of origin of $\{0\}$	$\boldsymbol{o}_1$	(0,0,0)
Position of strut mounting	$\boldsymbol{o}_2$	(0.136,0.497,0.011)
Initial position of $\boldsymbol{p}_5$	(p_{5x}, p_{5y}, p_{5z})	(-0.078,0.105,-0.108)
Initial position of $\boldsymbol{p}_8$	(p_{8x}, p_{8y}, p_{8z})	(0.434,-0.333,-0.019)
Euler angles relating$\{3\}$ to $\{0\}$	$(\beta_1, \beta_2, \beta_3)$	$\left(\frac{2\pi}{180}, \frac{\pi}{180}, \frac{-3\pi}{180}\right)$
Link-6 vector w.r.t.$\{2\}$	(l_{6x}, l_{6y}, l_{6z})	(-0.505,0.009,0.054)
Length of the knuckle	l_7	0.15
Distance between $\boldsymbol{p}_1$and $\boldsymbol{p}_3$	r	0.106
Distance between $\boldsymbol{p}_1$and $\boldsymbol{p}_6$	ρ	0.061
Mass of the lower-A arm	m_1	4.60 kg
Mass of the tie rod	m_4	1.0 kg
Mass of the (knuckle+ steering link)	m_2	12.1 kg
Equivalent mass of the (damper + spring)	m_3	4 kg
Un-stretched length of the suspension spring	l_0	0.4815
Mass of the tyre	m_5	25.0 kg

Table 3.2: Characteristics of suspension spring and damper (taken from [5]).

Stiffness (k_s)	4.22 E+04 N/m
Damping coefficient (c_s)	2.7 E+03 Ns/m

Table 3.3: Mass and inertia parameters of MPS (taken from [5]).

Body Description	Mass(in kg)	Inertia $(\mathrm{kg}-\mathrm{m}^2)$ (I_{xx}, I_{yy}, I_{zz})
Lower arm	4.6	0.1 ,0.1 ,0.1
Steering knuckle	12.1	0.25 ,0.25 ,0.25
Tie rod	1	0.1 ,0.1 ,0.1
Wheel	25	0.1 ,0.1 ,0.1

Table 3.4: Characteristics of the wheels (taken from [5]).

Radius (R)	0.35 m
Stiffness (k_t)	2.00 E+05 N/m
Damping coefficient $((c_t)$	8.0 E+04 Ns/m

3.2 Dynamic formulation in configuration space

The general equation of motion for rigid multi-body systems can be written as :

$$\boldsymbol{M}(\boldsymbol{q})\ddot{\boldsymbol{q}} + \boldsymbol{C}(\boldsymbol{q}, \dot{\boldsymbol{q}}) + \boldsymbol{G}(\boldsymbol{q}) = \boldsymbol{\tau}.$$

where, $\boldsymbol{q}$ represents the vector of configuration space variables. The significance of the terms $\boldsymbol{M}, \boldsymbol{C}$ and $\boldsymbol{G}$ and their physical interpretation has been explained in Chapter 2. The variables $\boldsymbol{q}$=$[\theta, l_2, c_1, c_2, c_3, s, x, y, z, \beta, \gamma]^\top$ define the full configuration space of the MacPherson strut suspension system. In our model, we have assumed our chassis to be fixed i.e. grounded. The wheel is analytically modelled as linear translational spring with damping characteristics. However, for exact modelling of the tyre, a complete non-linear model may be used which is not considered in this study because we are concerning only with the analysis of the suspension system. The suspension spring and damper has been included in the formulation of the dynamics in order to make the formulation more realistic and robust.

The steering knuckle is of constant length l_7 as given in Table 3.1 and on top of the steering knuckle, suspension spring and dampers are mounted and connected to $\boldsymbol{o}_2$ which is fixed to the chassis. The equivalent mass of the damper and spring has been replaced by a link of length $(l_2 - l_7)$ which varies as the road profile s and the steering input $\mathbf{y}$ vary.

The link 4, which is the steering link, is attached to the knuckle rigidly as shown in Fig. 3.1. As given in Table 3.1, m_2 is the total mass of steering link and knuckle. Therefore, in order to distribute mass individually to steering and knuckle for analysis, it is assumed that mass is directly proportional to length.

$$m_s = m_2 \frac{l_7}{l_7 + l_{4y}}$$

where, m_s is the mass of the steering link.

$$m_k = m_2 \frac{l_{4y}}{l_7 + l_{4y}}$$

where, m_k is the mass of the knuckle.

The formulation of the dynamics has been done in two parts:

1. Effect of spring has been included in the formulation of the dynamics.
2. Combined effect of spring and damper has been included in the formulation of the dynamics.

Addition of spring and damper will affect the $\boldsymbol{G}$ term of the formulation. Due to the addition of damper, a term $\frac{1}{2}c\dot{x}^2$ is added to the potential energy of the system. Basically, it is used to absorb the oscillation produced due to the road input $\mathbf{y}$ and the steering input s. As, it has been previously mentioned that in order to check the correctness of the formulation, energy check, zeroth order check and first order check has to be satisfied as described in the Section 2.4. Hence, the formulation has been divided into two parts and results have been reported for each of the case accordingly.

The $\boldsymbol{M}$ and $\boldsymbol{C}$ matrix can be computed for MacPherson strut suspension by referring to the method as described in Section 2.3.1.

The G matrix

The G matrix of the MPS suspension system can be calculated from the total potential energy of the system, V, which can written as:

$$V = \sum_{i=1}^{5} V_i$$

Potential energy of the system including the effect of spring has been mentioned below:

$$\begin{aligned}
V_1 =& \frac{1}{2} g l_1 m_1 \sin\theta, && (3.7)\\
V_2 =& \frac{1}{2(1+c_1^2+c_2^2+c_3^2)(m_k+m_s)} g m_2 (4 r c_1 c_2 m_k + 4 r c_3 m_k + 2 l_1 m_k \sin\theta \\
&+ 2\sin\theta c_1^2 l_1 m_k + 2 c_2^2 l_1 m_k \sin\theta + 2 c_3^2 l_1 m_k \sin\theta + 2 c_1 c_2 l_{4x} m_k + 2 c_3 l_{4x} m_k \\
&+ l_{4y} m_k - c_1^2 l_{4y} m_k + c_2^2 l_{4y} m_k - c_3^2 l_{4y} m_k - 2 c_1 l_{4z} m_k + 2 c_2 c_3 l_{4z} m_k \\
&+ 2 l_1 m_s \sin\theta + 2 c_1^2 l_1 m_s \sin\theta + 2 c_2^2 l_1 m_s \sin\theta + 2 c_3^2 l_1 m_s \sin\theta + 2 c_1 c_2 l_9 m_s \\
&+ 2 c_3 l_9 m_s), && (3.8)\\
V_3 =& \frac{1}{2} k_s (-l_2 + l_9 + l_s)^2 + g(l_1 \mathrm{sin}\theta + \frac{(c_1c_2+c_3)(l_2-l_9)}{1+c_1^2+c_2^2+c_3^2} + \frac{2(c_1c_2+c_3)l_9}{1+c_1^2+c_2^2+c_3^2}) m_3, \\
& && (3.9)\\
V_4 =& \frac{1}{2} g m_4 (s(\mathrm{cos}\beta_3 \mathrm{sin}\beta_1 \mathrm{sin}\beta_2 + \mathrm{cos}\beta_1 \mathrm{sin}\beta_3) + \frac{2r(c_1c_2+c_3)}{1+c_1^2+c_2^2+c_3^2} + l_1 \mathrm{sin}\theta \\
&+ \frac{2(c_1c_2+c_3)l_{4x}}{1+c_1^2+c_2^2+c_3^2} + \frac{(1-c_1^2+c_2^2-c_3^2)l_{4y}}{1+c_1^2+c_2^2+c_3^2} - \frac{2(c_1-c_2c_3)l_{4z}}{1+c_1^2+c_2^2+c_3^2} + p_{5y}), && (3.10)\\
V_5 =& \frac{1}{2} k_t (y - \frac{g m_5}{k_t})^2 + g m_5 (y + p_{8y}). && (3.11)
\end{aligned}$$

Due to the combined effect of spring and damper, there will be change in the V_3 and V_5. Addition of the term $\frac{1}{2} c_s \dot{l}_2^2$ and $\frac{1}{2} c_t \dot{y}^2$ on the right hand side of V_3 and V_5 will include the effect of damper characteristics in the system.

The Table 3.5. shows the size of $\mathbf{M}, \mathbf{C}$ and $\mathbf{G}$ matrices along with their dimensions.

Matrix	**Dimension**	Size (in KB)
$\boldsymbol{M}$	$12 \ \times 12$	1367
$\boldsymbol{C}$	$12 \ \times 12$	13289
$\boldsymbol{G}$	$12 \ \times 1$	60

Table 3.5: Size of $\boldsymbol{M}, \boldsymbol{C}$ and $\boldsymbol{G}$ matrices in analytical form along with their dimensions.

3.3 Assumption

1) The suspension system is freely falling under gravity, i.e. no external force or torque acting on the mechanical system,$\boldsymbol{\tau} = \mathbf{0}$.

2) The free-fall simulation of the MPS system has been conducted for a period of 2 seconds i.e. from t = 0 to 2 seconds.

3) In order to solve any differential equations, one require a set of initial conditions. For further analysis, the initial values of s and $\mathbf{y}$ have been assumed to be 0.05 m and 0.05 m respectively. Since, solving the dynamics problem in configuration space require the initial values of passive variables as well, therefore, their initial values will be calculated on the basis of assumed initial values of s and $\mathbf{y}$ as stated above using the forward kinematics as mentioned in the Chapter 2.

The initial set of conditions to solve the equation of motion in configuration space, i.e., $\boldsymbol{q} = [0.452, 0.388, -1.62, -2.52, 1.43, 0.050, -0.007, 0.050, -0.028, -0.055, 0.456]^\top$ and $\dot{\boldsymbol{q}} = \mathbf{0}$.

3.4 Method to solve the equation of motion in configuration space

The MacPherson system is reduced to a set of 11 simultaneous differential equations which is of the form as shown in Eq. (2.2). The set of 11 differential equations has to be solved in to understand the dynamics and behaviour of the system when applied with steering/rack input s and the road profile input $\mathbf{y}$. It is computationally very expensive and very difficult to solve the differential equations analytically. Therefore, a numerical approach to solving differential equations has been implemented. The problem to solving differential equation has been approached in two manner and has been explained in detailed version along with their respective computational time.

3.4.1 Method 1

The set of differential equation is solved numerically by implementing a numerical differentiator module using NDSolve in *Mathematica*. The flow chart in Fig. 3.2 describes the procedure.

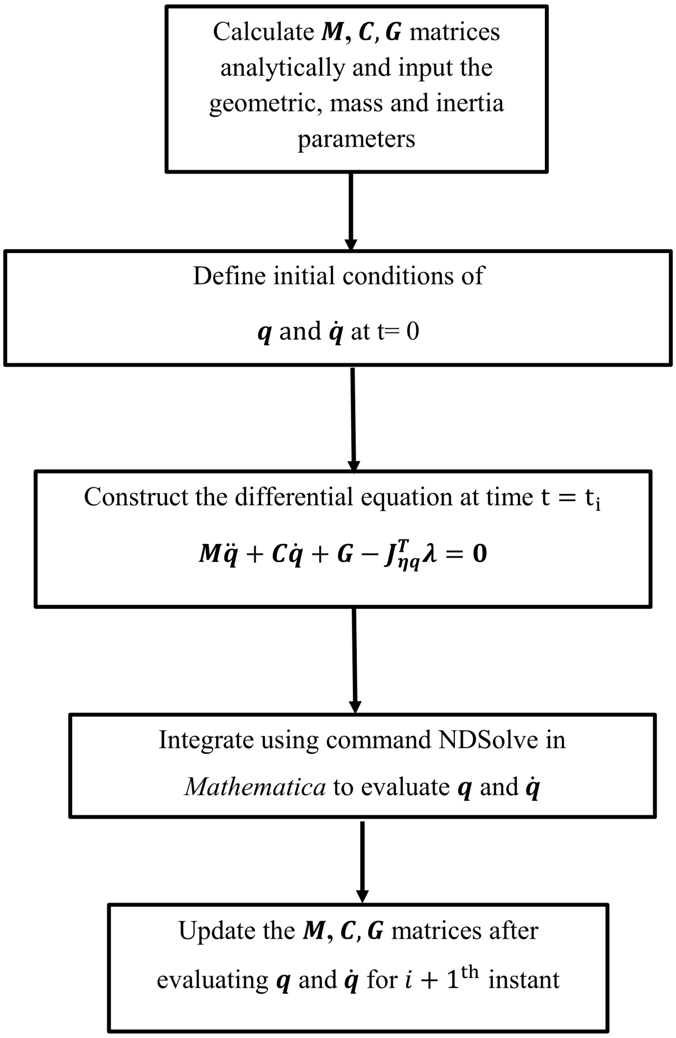

Figure 3.2: Flow chart for method 1.

The simulation was conducted for t = 0 to 2 seconds for a maximum of 10000 steps and the CPU run time taken to compute the solution was 7.71 minutes approximately.

3.4.2 Method 2

The set of differential equations is evaluated by implementing a numerical integrator module and solving the set of equations using Runge-Kutta fourth order method .The flow chart in Fig. 3.3 describes the procedure. The simulation is performed for t = 0 to 2 seconds for step size of h = 0.001. An error of the order 10^{-5} is observed compared to the solution obtained from method 1. Moreover, in terms of computation time taken to solve the system of differential equation, method 2 is more efficient compared to method 1. The CPU run time taken to compute the solution was 3.27 minutes. Computational efficiency of 57% is achieved in case of method 2.

In the Section 3.5 results obtained from method 2 have been presented along with the verifications that will validate the formulation of the MPS suspension system in configuration space.

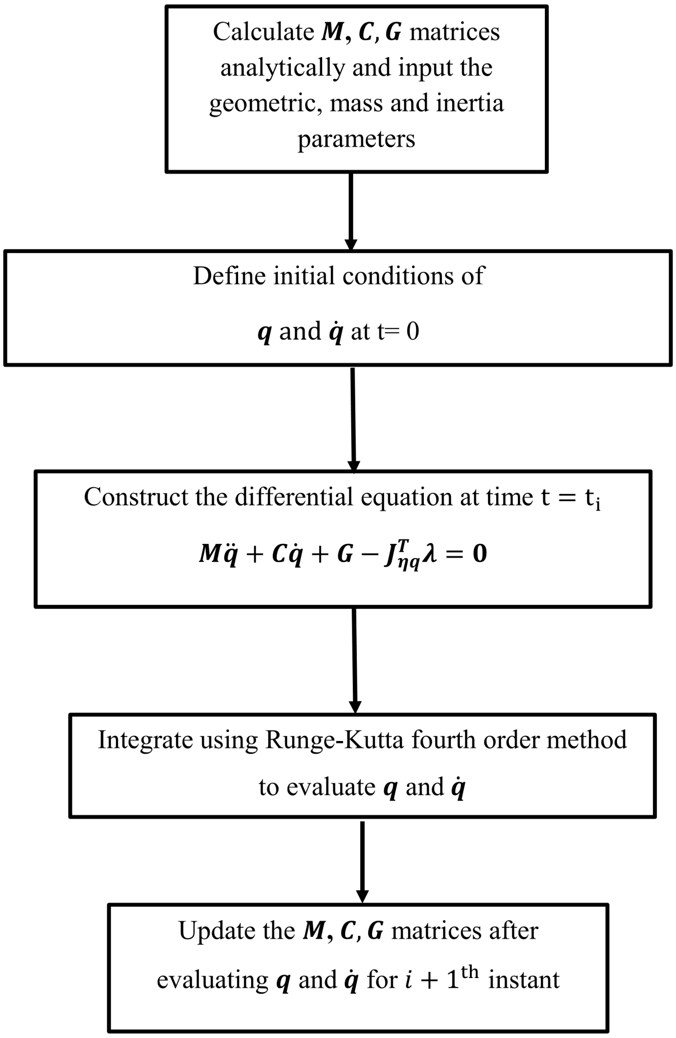

Figure 3.3: Flow chart for method 2.

3.5 Results of configuration space

3.5.1 Results when only spring is considered

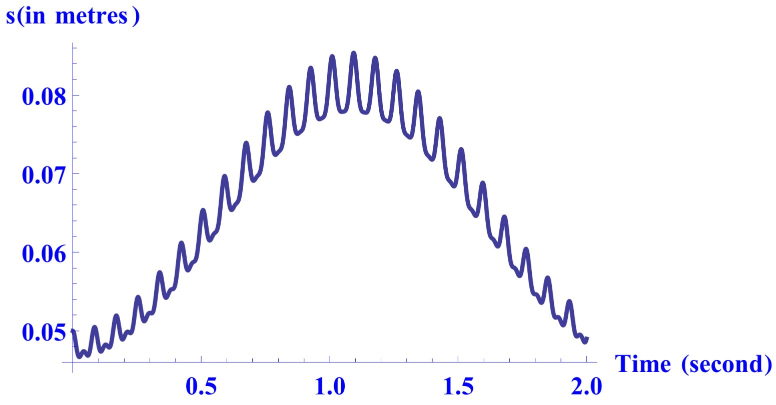

Figure 3.4: Variation of steering/rack input s with time.

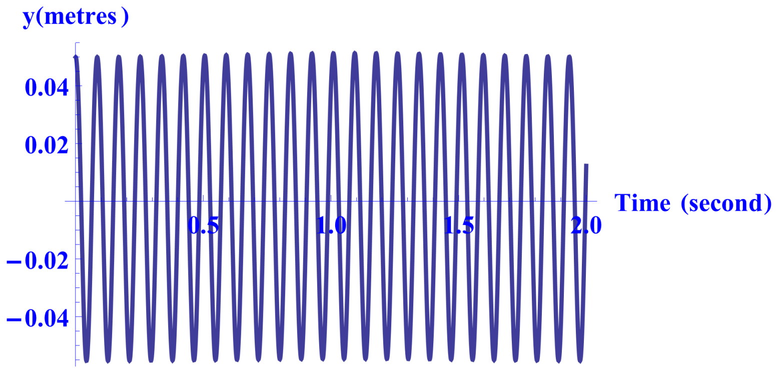

Figure 3.5: Variation of road profile input y with time.

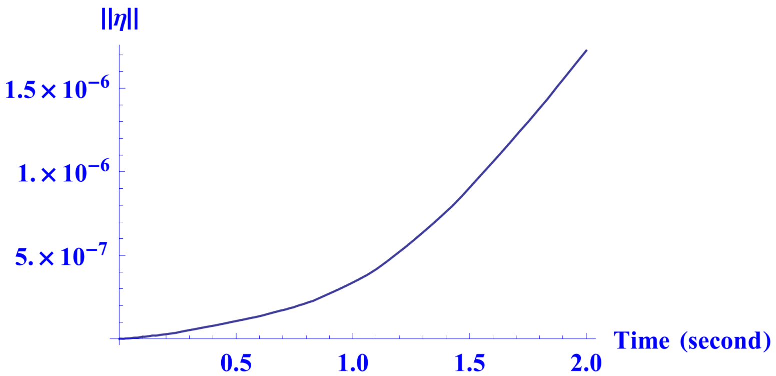

Figure 3.6: Variation of $||\eta||$ with time.

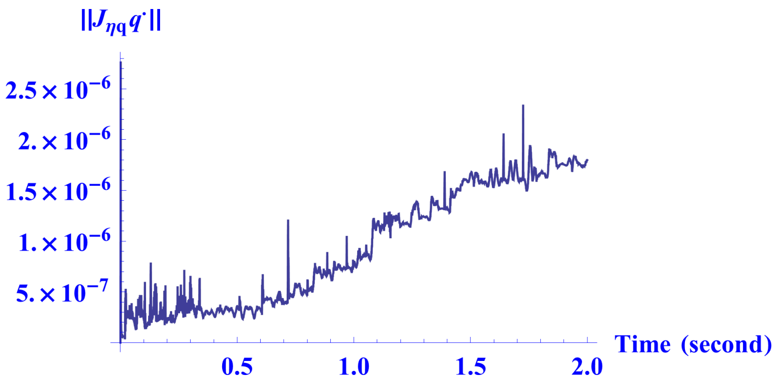

Figure 3.7: Variation of $\|\boldsymbol{J}_{\eta q}\dot{\boldsymbol{q}}\|$ with time.

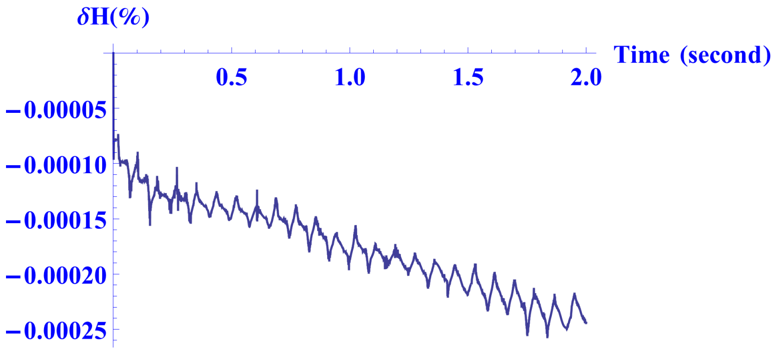

Figure 3.8: Percentage error in the conservation of total energy $\delta\mathbf{H}(\%)$ with time.

3.5.2 Results when spring and damper both are considered

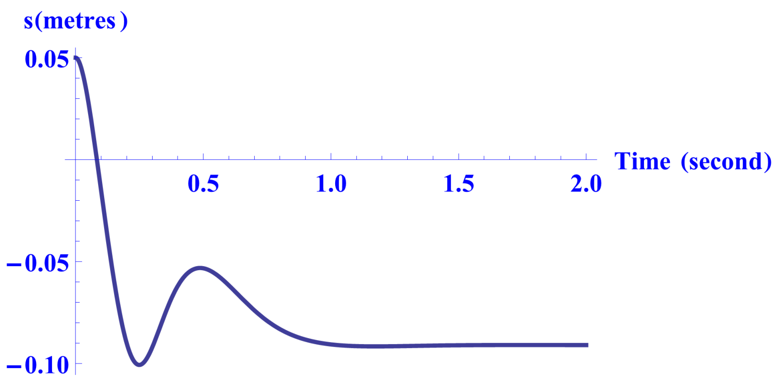

Figure 3.9: Variation of steering/rack input s with time.

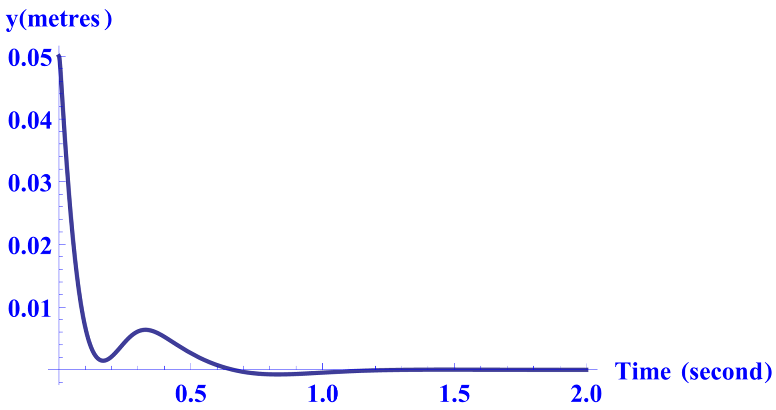

Figure 3.10: Variation of road profile input $\mathbf{y}$ with time.

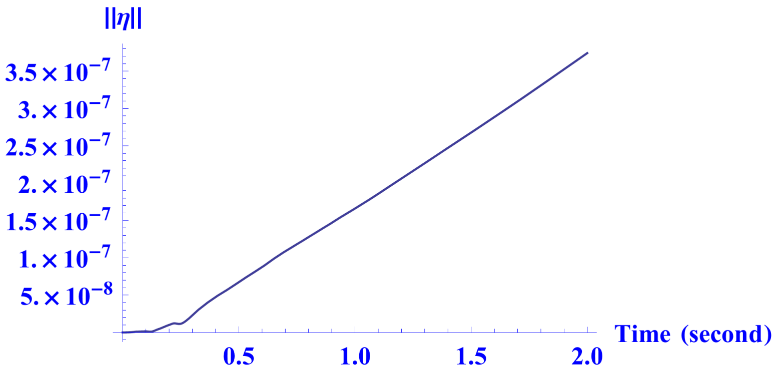

Figure 3.11: Variation of $||\boldsymbol{\eta}||$ with time.

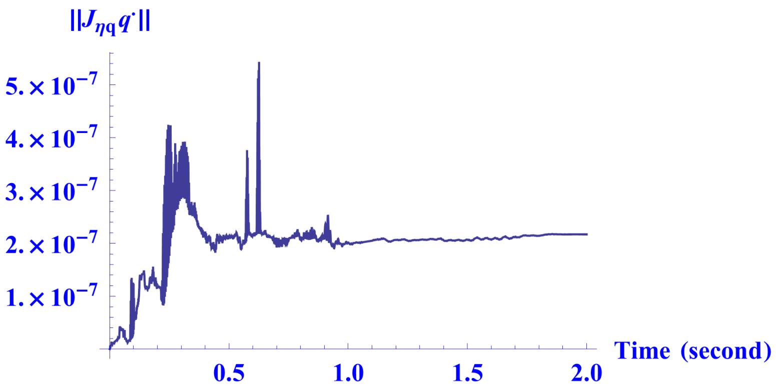

Figure 3.12: Variation of $\|\boldsymbol{J}_{\eta q}\dot{\boldsymbol{q}}\|$ with time.

3.6 Dynamic formulation in actuator space

The general equation of motion for rigid multi-body systems in actuator space can be written as:

$$\boldsymbol{M_\theta}\ddot{\boldsymbol{\theta}} + \boldsymbol{C_\theta}\dot{\boldsymbol{\theta}} + \boldsymbol{G_\theta} = \boldsymbol{\tau_\theta}, \tag{3.12}$$

Here, $\boldsymbol{\theta}$ represents the vector of active variables. The significance of the terms $\boldsymbol{M_\theta}$, $\boldsymbol{C_\theta}$ and $\boldsymbol{G_\theta}$ and their physical interpretation has been explained in the Chapter 2. The variables $\boldsymbol{\theta}$=$[s, y]^\top$ define the actuator space of the MacPherson strut suspension system, and are also termed as active variables. The variables which are dependent on active parameters are termed as inactive variables, $\boldsymbol{\phi}$=$[\theta, l_2, c_1, c_2, c_3, x, z, \beta, \gamma]^\top$. Therefore, in MPS suspension system, there are 2 active variables and 9 inactive variables. Using the approach described in Chapter 2, one can get the actuator space from full configuration space. The advantage of actuator space is that the number of differential equations to solve the equation of motion of the system is reduced. For example, in MacPherson suspension system, the set of differential equation is reduced from 11 to 2 in actuator space, i.e., the system is reduced to a 2×2 system. The $\boldsymbol{M_\theta}$, $\boldsymbol{C_\theta}$ and $\boldsymbol{G_\theta}$ matrices are quite complex in nature compared to $\boldsymbol{M}$, $\boldsymbol{C}$ and $\boldsymbol{G}$. Since, $\boldsymbol{M_\theta}$, $\boldsymbol{C_\theta}$ and $\boldsymbol{G_\theta}$ will be dependent on inactive variables, therefore the forward kinematics has to be solved at every time step to solve the system of differential equations.

As mentioned previously, the formulation of the dynamics has been done in two parts:

1. Effect of spring has been included in the formulation of the dynamics.
2. Combined effect of spring and damper has been included in the formulation of the dynamics.

3.7 Method to solve equation of motion in actuator space

The MacPherson system is reduced to a set of two simultaneous differential equations which is of the form as shown in Eq. (2.18). The set of two differential equations has to be solved in to understand the dynamics and behaviour of the system when applied with steering/rack input s and the road profile input y. It is computationally very expensive and very difficult to solve the differential equations analytically. Therefore, a numerical approach to solving differential equations has been implemented. The problem to solving differential equation has been approached in two manner and has been explained in detailed version along with their respective computational time.

3.7.1 Method 1

The set of differential equation is solved numerically by implementing a numerical integrator module using NDSolve in *Mathematica*. The flow chart in Fig. 3.13 describes the procedure. The simulation was conducted for t = 0 to t = 0.1 seconds with maximum number of steps 100 for the time interval. The computational time taken i.e. CPU run time to obtain the solution was approximately 16.04 hours, which is computationally quite expensive. In this approach, the functions $f_1(c_1, c_2, c_3) = 0,\ f_2(c_1, c_2, c_3) = 0, f_3(c_1, c_2, c_3) = 0$ were evaluated using Solve command in *Mathematica*, which takes approximately 5.6 minutes for evaluation every time-step. Moreover, upon observation it was found that NDSolve command in *Mathematica* takes multiple steps to converge to a solution for a single time-step leading to higher computational time.

3.7.2 Method 2

The set of differential equations is evaluated by implementing a numerical integrator module and solving the set of equations using Runge-Kutta fourth order method. The flow chart in Fig. 3.14 describes the procedure. The simulation is performed for t = 0 to 2 seconds for step size of h = 0.001. An error of the order 10^{-5} is observed compared to the solution obtained from configuration space. The CPU run time taken to compute the solution was 2.16 seconds to compute the solution. In this approach, the functions $f_1(c_1, c_2, c_3) = 0,\ f_2(c_1, c_2, c_3) = 0, f_3(c_1, c_2, c_3) = 0$ were evaluated numerically using Runge-Kutta fourth order method at every time step.

In the next Section 3.8, results obtained from method 2 have been presented along with the verifications that will validate the formulation of the MPS suspension system in actuator space.

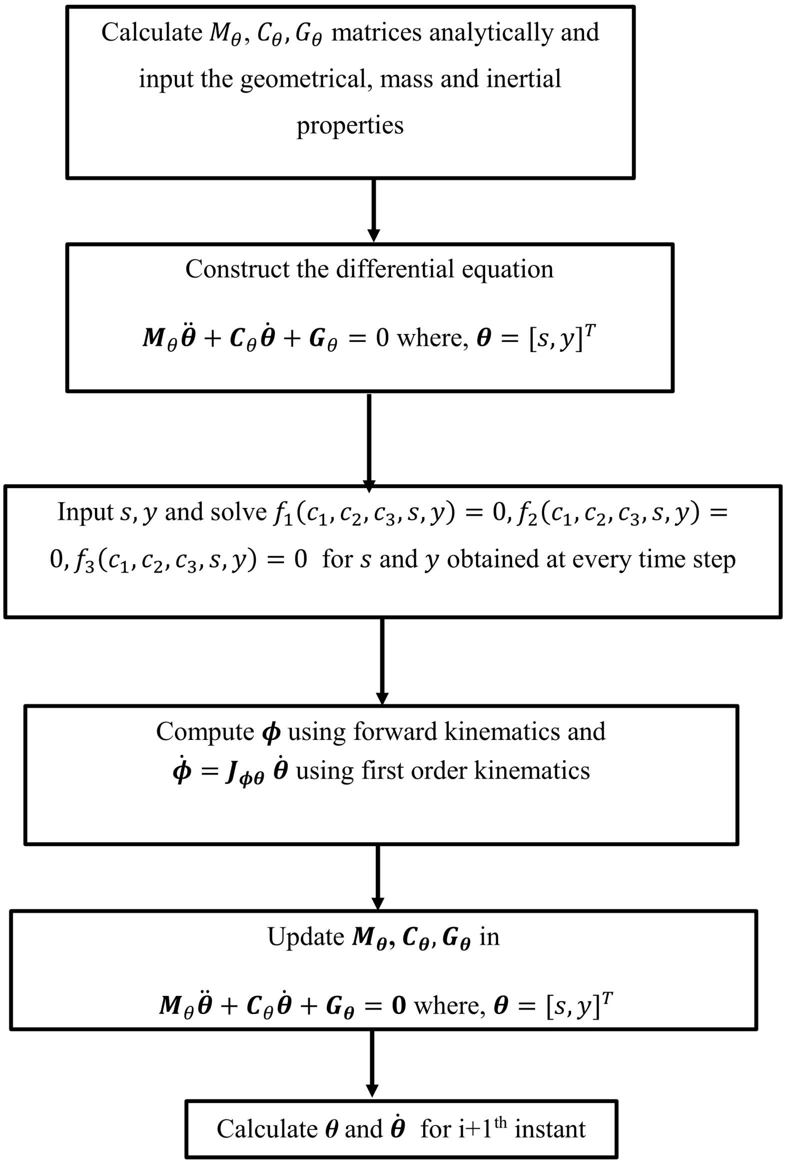

Figure 3.13: Flowchart for method 1.

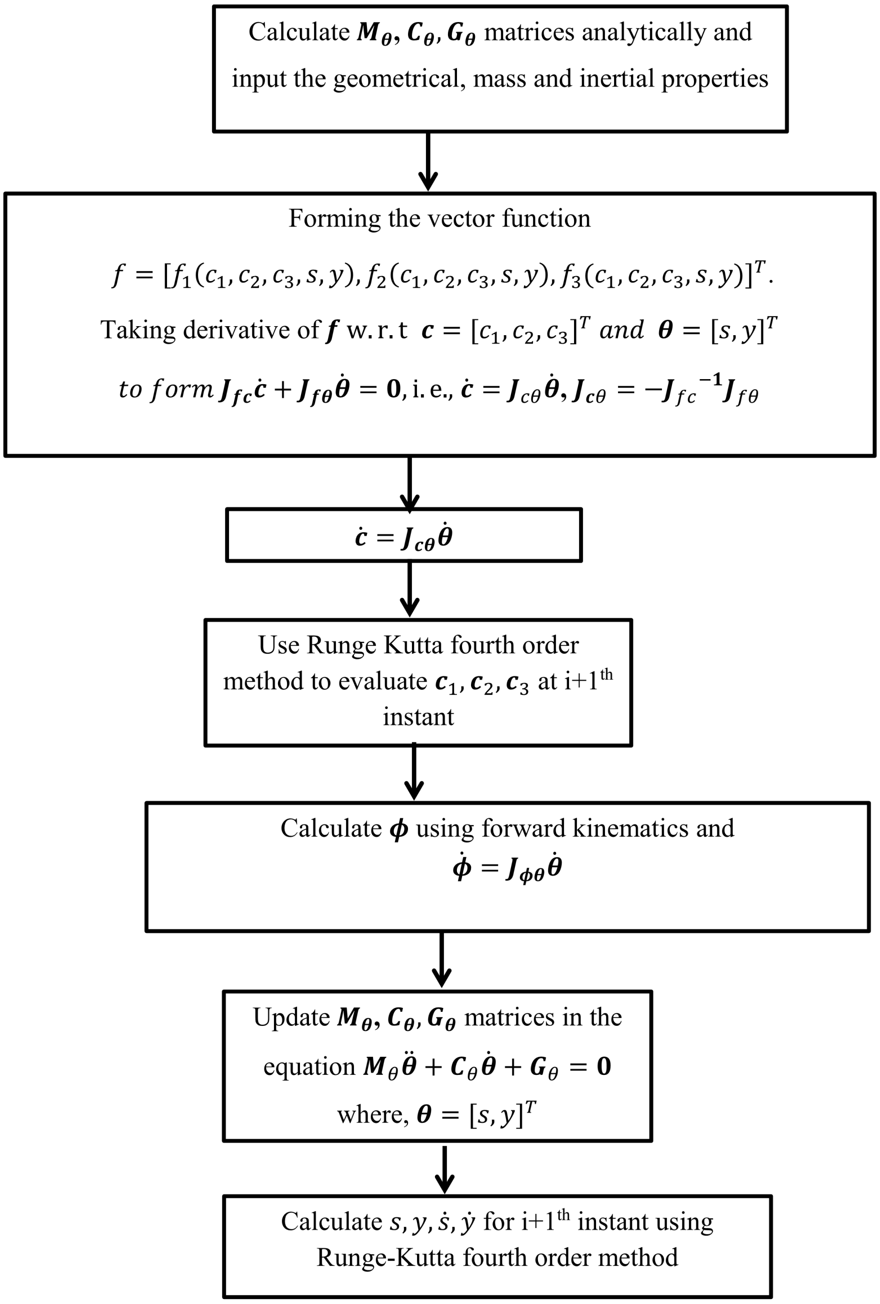

Figure 3.14: Flowchart for method 2.

3.8 Results of actuator space

3.8.1 Results when only spring is considered

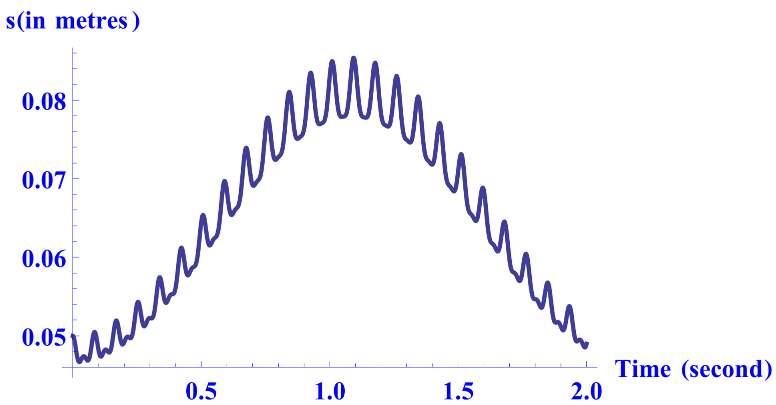

Figure 3.15: Variation of steering/rack input s with time.

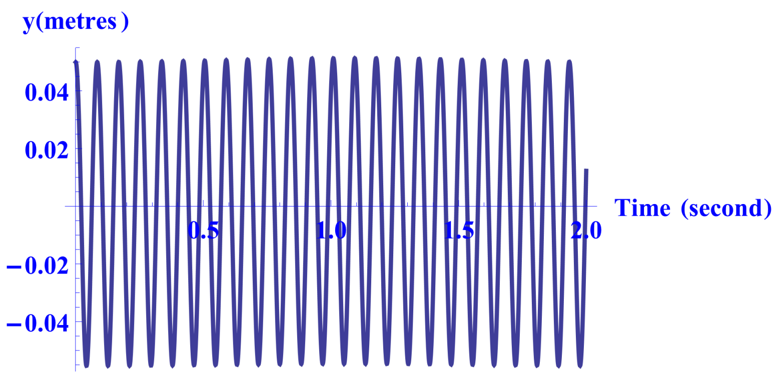

Figure 3.16: Variation of road profile input y with time.

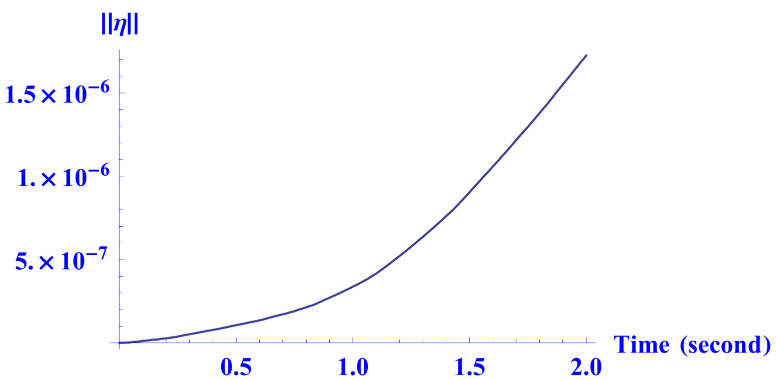

Figure 3.17: Variation of $||\eta||$ with time.

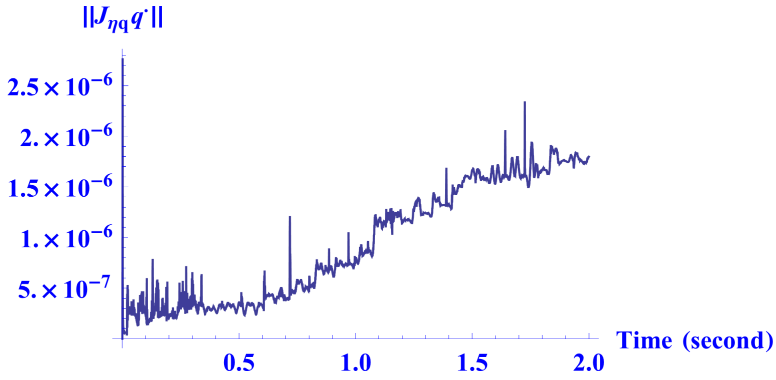

Figure 3.18: Variation of $\|\boldsymbol{J}_{\eta q}\dot{\boldsymbol{q}}\|$ with time.

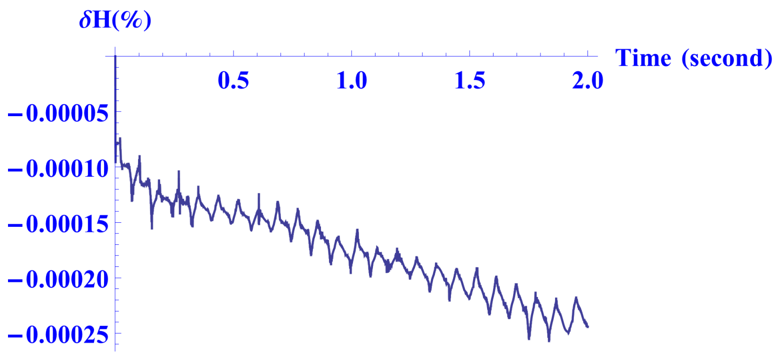

Figure 3.19: Percentage error in the conservation of total energy $\delta\mathrm{H}(\%)$ with time.

3.8.2 Results when spring and damper both are considered

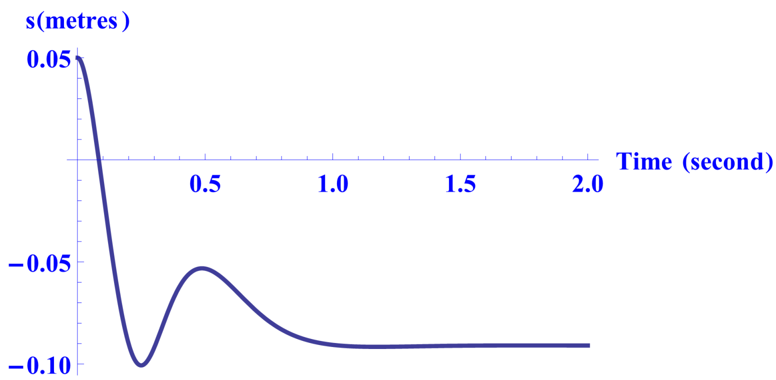

Figure 3.20: Variation of steering/rack input s with time.

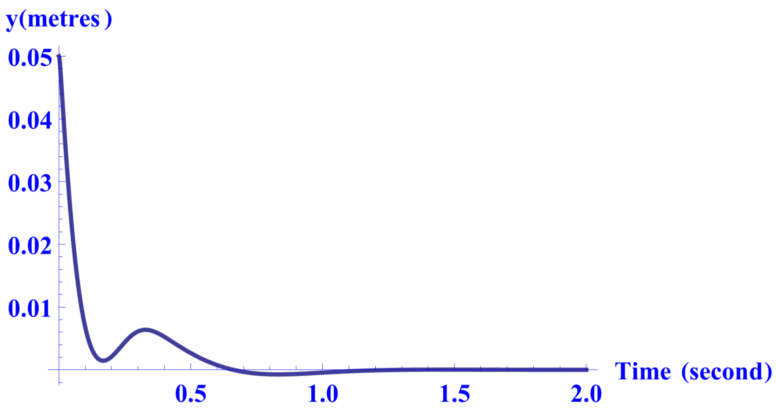

Figure 3.21: Variation of road profile input $\mathbf{y}$ with time.

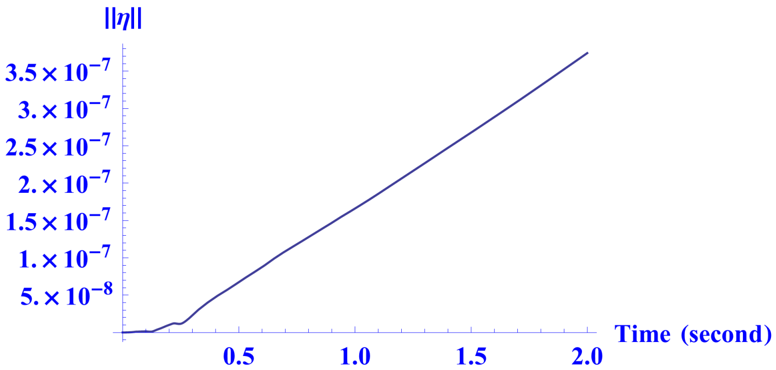

Figure 3.22: Variation of $||\boldsymbol{\eta}||$ with time.

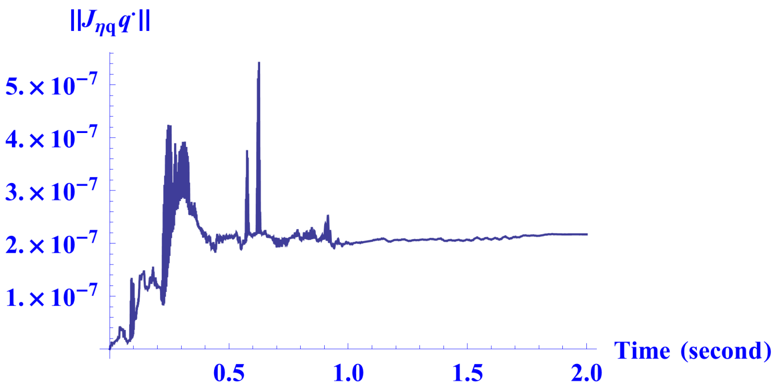

Figure 3.23: Variation of $\|\boldsymbol{J}_{\eta q}\dot{\boldsymbol{q}}\|$ with time.

CHAPTER 4

DYNAMIC FORMULATION OF DOUBLE WISHBONE SUSPENSION

Spatial kinematic model of double wishbone suspension as presented in a work by Madhu Kodati (see [1]) is used in the formulation of the equation of dynamics. Details of the kinematic model has been included in the first part of this chapter for the sake of completeness. Later, the formulation for the dynamics of the double wishbone suspension system has been presented with validations to check the correctness of the formulation.

4.1 Kinematic model

A comprehensive spatial kinematic model of double wishbone has been presented in this section.

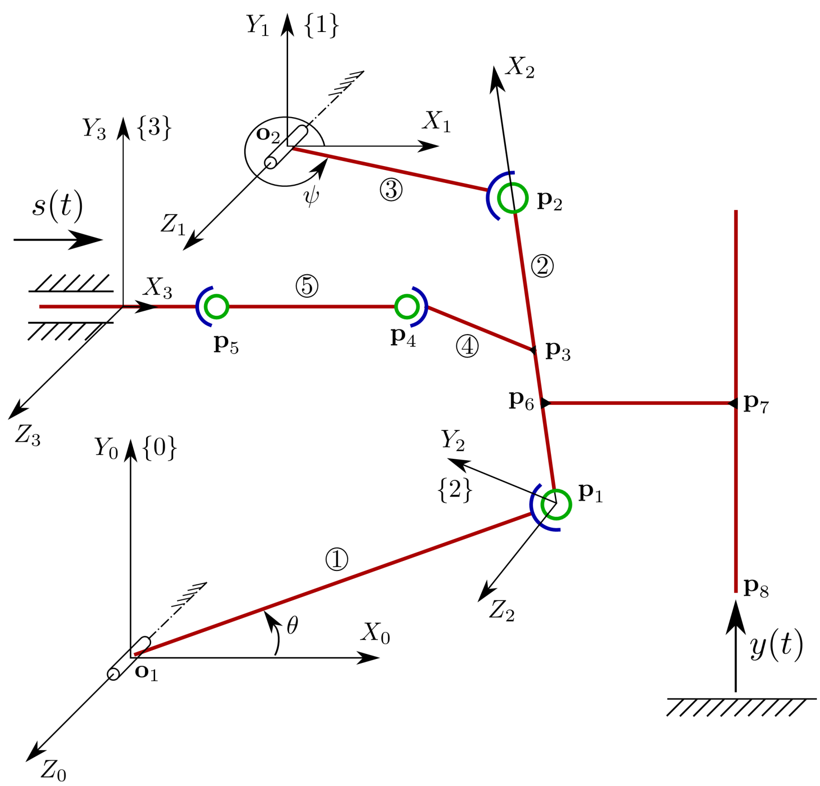

Figure 4.1: Kinematic model of double wishbone mechanism (taken from [1]).

The schematic model of DWB suspension is as shown in Fig. 4.1. Kinematically, it is a combination of spatial four-bar mechanism $\boldsymbol{o}_1\boldsymbol{p}_1\boldsymbol{o}_2\boldsymbol{o}_1$ with the chassis as the ground link, king-pin as the coupler and a spatial five-bar mechanism $\boldsymbol{o}_1\boldsymbol{p}_1\boldsymbol{p}_4\boldsymbol{p}_5\boldsymbol{o}_1$. These two mechanism are coupled at the king-pin.

Three co-ordinate systems are used to define the system. The global frame of reference $\{0\}$ is attached to $\boldsymbol{o}_1$, and its Z_0-axis is aligned to the axis of the hinges of the lower A-arm. Link-1 moves in the X_0Y_0 plane. Two body- fixed frames of reference, namely $\{1\}$ and $\{2\}$, are attached to the point $\boldsymbol{o}_2$ and $\boldsymbol{p}_1$ respectively. The Z_1-axis of $\{1\}$ is aligned to the axis of the hinges of upper-A arm and link-3 is confined in the X_1Y_1 plane. The link-2 lies in the plane X_2Y_2 and X_2 axis lies along the vector $(\boldsymbol{p}_2 - \boldsymbol{p}_1)$.

The rotation matrix ${}^0_3\mathbf{R}$ relating the orientation of frame $\{3\}$ to $\{0\}$ has been parameterized in terms of $XYZ\ Euler\ angles,\ (\beta_1,\ \beta_2, \beta_3)$(see [3]).

$$ {}^{\mathbf{0}}_{\mathbf{3}}\mathbf{R} = \mathbf{R}_X(\beta_1)\mathbf{R}_Y(\beta_2)\mathbf{R}_Z(\beta_3). \tag{4.1} $$

The rotation matrix ${}^0_1\mathbf{R}$ relating the orientation of frame $\{2\}$ to $\{0\}$ has been parameterized in terms of $XYZ\ Euler\ angles,\ (\alpha_1,\ \alpha_2, \alpha_3)$.

$$ {}^0_1\mathbf{R} = \mathbf{R}_X(\alpha_1)\mathbf{R}_Y(\alpha_2)\mathbf{R}_Z(\alpha_3). \tag{4.2} $$

Simlarily, the rotation matrix ${}^0_2\mathbf{R}$ relating the orientation of frame $\{2\}$ to $\{0\}$ has been parameterized in terms of Rodrigue's parameters, $\mathbf{c}$=$[c_1, c_2, c_3]^\top \in R^{\,3}$ (see [3]).

In order to formulate the dynamics of double wishbone suspension system, we need to incorporate the effect of suspension spring and damper. The suspension spring is connected to the chassis by a spherical joint and to the lower-A arm by a revolute joint as shown in Fig. 1.1. The spring leg is placed on the lower-A arm at a distance l_s from $\boldsymbol{o}_1$ along the link 1. The joint between $\boldsymbol{p}_7$ and $\boldsymbol{o}_3$ is a translational joint.

The rotation matrix ${}^0_4\mathbf{R}$ relating the orientation of $\{4\}$ to $\{0\}$, i.e, the orientaion of spring leg w.r.t. global reference of frame $\{0\}$. The spring leg is attached in such a way that it makes δ_1 with *X* -axis and δ_2 with the *Z*- axis of reference frame $\{0\}$.

$$ {}^{0}_{4}\boldsymbol{R}{=}\boldsymbol{R}_{Y}(\beta)\boldsymbol{R}_{Z}(\gamma). \tag{4.3}$$

On top of the spring leg, suspension spring and damper are mounted and attached to the fixed chassis at $\mathbf{o}_3$ by spherical joint.

4.1.1 Formulation of the loop - closure equations

The loop closure equation as obtained in Eq. (A.31) can be represented as:

$$\boldsymbol{p}_4{-}\boldsymbol{p}_5{-}{}^{0}_{4}\boldsymbol{R}[l_5,0,0]^{\top}{=}\mathbf{0}. \tag{4.4}$$

where,

$$ {}^{0}_{4}\boldsymbol{R}{=}\boldsymbol{R}_{Y}(\beta)\boldsymbol{R}_{Z}(\gamma). \tag{4.5}$$

β and γ are the *Euler-angle* of the tie-rod about the *Y*-axis and *Z*-axis of the global reference frame $\{0\}$.

The Eq. (4.4) can be written as:

$$\boldsymbol{\eta}_4 = [\eta_{4x},\ \eta_{4y}, \eta_{4z}]^{\top}, \tag{4.6}$$

$$\begin{aligned}\eta_{4x} = &- s\cos\beta_2\cos\beta_3 + l_1\cos\theta + \frac{r\,(1+c_1^2-c_2^2-c_3^2)\,l_2}{1+c_1^2+c_2^2+c_3^2} - l_5\cos\beta\cos\gamma\\ &+ \frac{(1+c_1^2-c_2^2-c_3^2)\,l_{4x}}{1+c_1^2+c_2^2+c_3^2} + \frac{(2c_1c_2-2c_3)\,l_{4y}}{1+c_1^2+c_2^2+c_3^2} + \frac{2\,(c_2+c_1c_3)\,l_{4z}}{1+c_1^2+c_2^2+c_3^2} - p_{5x},\end{aligned} \tag{4.7}$$

$$\begin{aligned}\eta_{4y} = &-s\,(\cos\beta_3\sin\beta_1\sin\beta_2 + \cos\beta_1\sin\beta_3) + l_1\sin\theta + \frac{2r\,(c_1c_2+c_3)\,l_2}{1+c_1^2+c_2^2+c_3^2} - l_5\sin\gamma\\ &+ \frac{2\,(c_1c_2+c_3)\,l_{4x}}{1+c_1^2+c_2^2+c_3^2} + \frac{(1-c_1^2+c_2^2-c_3^2)\,l_{4y}}{1+c_1^2+c_2^2+c_3^2} - \frac{2\,(c_1-c_2c_3)\,l_{4z}}{1+c_1^2+c_2^2+c_3^2} - p_{5y},\end{aligned} \tag{4.8}$$

$$\eta_{4z} = -s\left(-\cos\beta_1 \cos\beta_3 \sin\beta_2 + \sin\beta_1 \sin\beta_3\right) + \frac{2r\left(-c_2 + c_1 c_3\right) l_2}{1 + c_1^2 + c_2^2 + c_3^2} + l_5 \cos\gamma \sin\beta$$
$$+ \frac{2\left(-c_2 + c_1 c_3\right) l_{4x}}{1 + c_1^2 + c_2^2 + c_3^2} + \frac{2\left(c_1 + c_2 c_3\right) l_{4y}}{1 + c_1^2 + c_2^2 + c_3^2} + \frac{\left(1 - c_1^2 - c_2^2 + c_3^2\right) l_{4z}}{1 + c_1^2 + c_2^2 + c_3^2} - p_{5z}, \quad (4.9)$$

The loop-closure equation obtained from the loop $\boldsymbol{o}_1 \boldsymbol{p}_7 \boldsymbol{o}_3 \boldsymbol{o}_1$ can be expressed as:

$$\boldsymbol{o}_1 + \mathbf{R}_z\left(\theta\right)\left[l_1, 0, 0\right]^\top + {}^{\mathbf{0}}_{\mathbf{4}}\mathbf{R}[l_6, 0, 0]^\top - \boldsymbol{o}_3 = \mathbf{0}. \quad (4.10)$$

The expression on the left hand side of Eq. (4.10) can be written in the form

$$\boldsymbol{\eta}_5 = \left[\eta_{5x},\ \eta_{5y}, \eta_{5z}\right]^\top, \quad (4.11)$$

$$\eta_{5x} = l_8 \cos\delta_2 + l_s \cos\theta - o_{3x}, \quad (4.12)$$

$$\eta_{5y} = l_8 \cos\delta_1 \sin\delta_2 + l_s \sin\theta - o_{3y}, \quad (4.13)$$

$$\eta_{5z} = l_8 \sin\delta_1 \sin\delta_2 - o_{3z}. \quad (4.14)$$

Therefore, the constraint set of equations used in the formulation of dynamics can be expressed as: $\boldsymbol{\eta} = \left[\eta_{1x}, \eta_{1y}, \eta_{1z}, \eta_{3x}, \eta_{3y}, \eta_{3z}, \eta_{4x}, \eta_{4y}, \eta_{4z}, \eta_{5x}, \eta_{5y}, \eta_{5z}\right]^\top$.

The constraint equations $\eta_{1x}, \eta_{1y}, \eta_{1z}, \eta_{3x}, \eta_{3y}, \eta_{3z}$ are presented in detail in Section A.2 (taken from [1]).

Table 4.1: Geometric and mass values (taken from [4], with minor modifications).

Parameter	**Symbol**	**Value**
Length of lower-A arm	l_1	0.420
Length of tie rod	l_5	0.519
Length of upper-A arm	l_3	0.260
Length of the knuckle	l_2	0.163
Link-4vector w.r.t.$\{2\}$	(l_{4x}, l_{4y}, l_{4z})	(0,0.103,0)
Position of origin of $\{0\}$	$\boldsymbol{o}_1$	(0,0,0)
Position of origin of $\{1\}$	$\boldsymbol{o}_2$	(0.130,0.160,0)
Position of strut mounting	$\boldsymbol{o}_3$	(0.136,0.497,0.011)
Initial position of $\boldsymbol{p}_5$	(p_{5x}, p_{5y}, p_{5z})	(0.010,0.020,-0.4)
Initial position of $\boldsymbol{p}_8$	(p_{8x}, p_{8y}, p_{8z})	(0.480,-0.050,0)
Euler angles relating$\{3\}$ to $\{0\}$	$(\beta_1, \beta_2, \beta_3)$	$\left(\frac{2\pi}{180}, \frac{\pi}{180}, \frac{-3\pi}{180}\right)$
Euler angles relating$\{1\}$ to $\{0\}$	$(\alpha_{\mathbf{1}}, \alpha_{\mathbf{2}}, \alpha_{\mathbf{3}})$	$\left(\frac{-2\pi}{180}, \frac{-\pi}{180}, \frac{3\pi}{180}\right)$
Link-6 vector w.r.t.$\{2\}$	(l_{6x}, l_{6y}, l_{6z})	(-0.209,0.007-,0.030)
$\|\boldsymbol{p}_1 - \boldsymbol{p}_3\|$ as a fraction of l_2	r	0.473
$\|\boldsymbol{p}_1 - \boldsymbol{p}_6\|$ as a fraction of l_2	ρ	0.312
Length of the spring leg	l_7	0.15
Mass of the lower and upper-A arm	m_1	1 kg
Mass of the tie rod	m_4	1 kg
Mass of the (knuckle+ steering link)	m_2	8 kg
Equivalent mass of the (damper + spring)	m_3	4 kg
Un-stretched length of the suspension spring	l_0	0.4815
Mass of the tyre	m_5	22 kg
Mass of the spring leg	m_6	2 kg

Table 4.2: Characteristics of suspension spring and damper (taken from [4]).

Stiffness (k_s)	5.11 E+04 N/m
Damping coefficient (c_s)	1.44 E+04 Ns/m

Table 4.3: Mass and inertia parameters (taken from [4]).

Body Description	Mass(in kg)	Inertia (kgm^2)(I_{xx}, I_{yy}, I_{zz})
Lower and upper arm	1.0	0.028 ,0.02 ,0.03
Steering knuckle	8.0	1.6,1.6,1.6
Tie rod	1.0	0.1 ,0.1 ,0.1
Wheel	22.0	2.0,1.35,2.0

Table 4.4: Characteristics of the wheel (taken from [4]).

Radius (R)	0.35 m
Stiffness (k_t)	3 E+05 N/m
Damping coefficient ((c_t)	0.1 E+04 Ns/m

4.2 Dynamic formulation in configuration space

The general equation of motion for rigid multi-body systems can be written as :

$$\boldsymbol{M}(\boldsymbol{q})\ddot{\boldsymbol{q}} + \boldsymbol{C}(\boldsymbol{q}, \dot{\boldsymbol{q}}) + \boldsymbol{G}(\boldsymbol{q}) = \boldsymbol{\tau}.$$

where, $\boldsymbol{q}$ represents the vector of configuration space variables. The significance of the terms $\boldsymbol{M}$**,** $\boldsymbol{C}$ and $\boldsymbol{G}$ and their physical interpretation has been explained in the Chapter 2. The variables $\boldsymbol{q}$=$[\theta, \psi, c_1, c_2, c_3, s, x, y, z, \beta, \gamma, \delta_1, \delta_2]^\top$, define the full configuration space of the MacPherson strut suspension system. In our model, we have assumed our chassis to be fixed i.e. grounded. The wheel is analytically modelled as linear translational spring with damping characteristics. However, for exact modeling of the tyre, a complete non-linear model may be used which is not considered in this study because we are concerning only with the analysis of the suspension system. The suspension spring and damper has been included in the formulation of the dynamics in order to make the formulation more realistic and robust.

The steering knuckle is of constant length l_2 as given in Table 4.1. The link 4, which is the steering link, is attached to the knuckle rigidly as shown in Fig. 4.1. As given in Table 4.1, m_2 is the total mass of steering link and knuckle. Therefore, in order to distribute mass individually to steering and knuckle for analysis, it is assumed that mass is directly proportional to length.

$$m_s = m_2 \frac{l_2}{l_2 + l_{4y}}$$

where, m_s is the mass of the steering link.

$$m_k = m_2 \frac{l_{4y}}{l_2 + l_{4y}}$$

where, m_k is the mass of the knuckle.

The formulation of the dynamics has been done in two parts:

1. Effect of spring has been included in the formulation of the dynamics.
2. Combined effect of spring and damper has been included in the formulation of the dynamics.

Addition of spring and damper will affect the $\boldsymbol{G}$ term of the formulation. Due to the addition of damper, a term $\frac{1}{2}c\dot{x}^2$ is added to the potential energy of the system. Basically, it is used to absorb the oscillation produced due to the road input $\mathbf{y}$ and the steering input $\mathbf{s}$. As, it has been previously mentioned that in order to check the correctness of the formulation, energy check, zeroth order check and first order check has to be satisfied as described in the Section 2.4. Hence the formulation has been divided into two parts and results have been reported for each of the case accordingly.

The $\boldsymbol{M}$ and $\boldsymbol{C}$ matrices can be computed for double wishbone suspension by referring to the method as described in Section 2.3.1.

The $\boldsymbol{G}$ matrix

The $\boldsymbol{G}$ matrix of the MPS suspension system can be calculated from the total potential energy of the system, V, which can written as:

$$V = \sum_{i=1}^{7} V_i$$

Potential energy of the system including the effect of spring has been mentioned below:

$$
\begin{aligned}
V_1 =& \frac{1}{2} g l_1 m_1 \text{sin}\theta, \qquad (4.15)\\
V_2 =& \frac{1}{m_k + m_s} g m_2 (\frac{1}{2}(2 l_1 \text{sin}\theta + \frac{4r(c_1 c_2 + c_3) l_2}{1 + c_1^2 + c_2^2 + c_3^2} + \frac{2(c_1 c_2 + c_3) l_{4x}}{1 + c_1^2 + c_2^2 + c_3^2} \\
&+ \frac{(1 - c_1^2 + c_2^2 - c_3^2) l_{4y}}{1 + c_1^2 + c_2^2 + c_3^2} - \frac{2(c_1 - c_2 c_3) l_{4z}}{1 + c_1^2 + c_2^2 + c_3^2}) m_s \\
&+ \frac{1}{2} m_k (l_2 (\text{cos}\psi(\text{cos}\alpha_3 \text{sin}\alpha_1 \text{sin}\alpha_2 + \text{cos}\alpha_1 \text{sin}\alpha_3) \\
&+ \text{sin}\psi(\text{cos}\alpha_1 \text{cos}\alpha_3 - \text{sin}\alpha_1 \text{sin}\alpha_2 \text{sin}\alpha_3)) + l_1 \text{sin}\theta + o_{2y})), \qquad (4.16)\\
V_3 =& g m_3 (\frac{1}{2} l_3 (\text{cos}\psi(\text{cos}\alpha_3 \text{sin}\alpha_1 \text{sin}\alpha_2 + \text{cos}\alpha_1 \text{sin}\alpha_3) + \text{sin}\psi(\text{cos}\alpha_1 \text{cos}\alpha_3 \\
&- \text{sin}\alpha_1 \text{sin}\alpha_2 \text{sin}\alpha_3)) + o_{2y}), \qquad (4.17)\\
V_4 =& \frac{1}{2} g m_4 (s(\text{cos}\beta_3 \text{sin}\beta_1 \text{sin}\beta_2 + \text{cos}\beta_1 \text{sin}\beta_3) + l_1 \text{sin}\theta + \frac{2r(c_1 c_2 + c_3) l_2}{1 + c_1^2 + c_2^2 + c_3^2} \\
&+ \frac{2(c_1 c_2 + c_3) l_{4x}}{1 + c_1^2 + c_2^2 + c_3^2} + \frac{(1 - c_1^2 + c_2^2 - c_3^2) l_{4y}}{1 + c_1^2 + c_2^2 + c_3^2} - \frac{2(c_1 - c_2 c_3) l_{4z}}{1 + c_1^2 + c_2^2 + c_3^2} + p_{5y}), \qquad (4.18)\\
V_5 =& \frac{1}{2} k_t (y - \frac{g m_5}{k_t})^2 + g m_5 (R + y + p_{8y}), \qquad (4.19)\\
V_6 =& g m_6 (\frac{1}{2} \text{cos}\delta_1 \text{sin}\delta_2 (l_8 - l_9) + l_9 \text{cos}\delta_1 \text{sin}\delta_2 + l_s \text{sin}\theta), \qquad (4.20)\\
V_7 =& \frac{1}{2} k_s (-l_8 + l_9 + l_s)^2 + g m_3 (\frac{1}{2} l_9 \text{cos}\delta_1 \text{sin}\delta_2 + l_s \sin\theta). \qquad (4.21)
\end{aligned}
$$

Due to the combined effect of spring and damper, there will be change in the V_3 and V_5. Addition of the term $\frac{1}{2} c_s \dot{l}_2^2$ and $\frac{1}{2} c_t \dot{y}^2$ on the right hand side of V_7 and V_5 will include the effect of damper characteristics in the system respectively.

The Table 4.5 shows the size of $\boldsymbol{M}$, $\boldsymbol{C}$ and $\boldsymbol{G}$ matrices in analytical form along with their dimensions.

Table 4.5: Size of $\boldsymbol{M}, \boldsymbol{C}$ and $\boldsymbol{G}$ matrices along with their dimensions.

Matrix	**Dimension**	Size (in KB)
$\boldsymbol{M}$	14 $\times$ 14	1160
$\boldsymbol{C}$	14 $\times$ 14	8214
$\boldsymbol{G}$	14 $\times$ 1	49

4.3 Assumption

1) The suspension system is freely falling under gravity, i.e. no external force or torque acting on the mechanical system,$\boldsymbol{\tau} = \mathbf{0}$.

2) The free- fall simulation of the DWB system has been conducted for a period of 2 seconds i.e. from t = 0 to 2 seconds.

3) In order to solve any differential equations, one require a set of initial conditions. For further analysis, the initial values of s and $\mathbf{y}$ have been assumed to be 0.05 m and 0.05 m respectively. Since, solving the dynamics problem in configuration space require the initial values of passive variables as well , therefore, their initial values will be calculated on the basis of assumed initial values of s and $\mathbf{y}$ as stated above using the forward kinematics as mentioned in the Chapter 2.

The initial set of conditions to solve the equation of motion in configuration space, i.e., $\boldsymbol{q}$ = $[0.348, 0.515, -1.66, -2.21, 1.34, 0.050, -0.011, 0.050, 0.008, -0.710, 0.421, 0.422, 0.030, 1.97]^\top$ and $\dot{\boldsymbol{q}} = \mathbf{0}$.

4.4 Method to solve the equation of motion in configuration space

The double wishbone suspension system is reduced to a set of 14 simultaneous differential equations which is of the form as shown in Eq. (2.2). The set of 14 differential equations has to be solved in to understand the dynamics and behaviour of the system when applied with steering/rack input s and the road profile input $\mathbf{y}$. It is computationally very expensive and very difficult to solve the differential equations analytically. Therefore, a numerical approach to solving differential equations has been implemented. The problem to solving differential equation has been approached in two manner and has been explained in detailed version along with their respective computational time.

4.4.1 Method 1

The set of differential equation is solved numerically by implementing a numerical differentiator module using NDSolve in *Mathematica*. The flow chart in Fig. (3.2) describes the procedure.

The simulation was conducted for t = 0 to 2 seconds for a maximum of 10000 steps and the CPU run time taken to compute the solution was 11.63 minutes approximately.

4.4.2 Method 2

The set of differential equations is evaluated by implementing a numerical integrator module and solving the set of equations using Runge-Kutta fourth order method. The flow chart in Fig. (3.3) describes the procedure. The simulation is performed for t = 0 to 2 seconds for step size of h = 0.001. An error of the order 10^{-5} is observed compared to the solution obtained from method 1. Moreover, in terms of computation time taken to solve the system of differential equation, method 2 is more efficient compared to method 1. The CPU run time taken to compute the solution was 6.28 minutes. Computational efficiency of 46% is achieved in case of method 2.

In the Section 4.5, results obtained from method 2 have been presented along with the verifications that will validate the formulation of the DWB suspension system in configuration space.

4.5 Results of configuration space

4.5.1 Results when only spring is considered

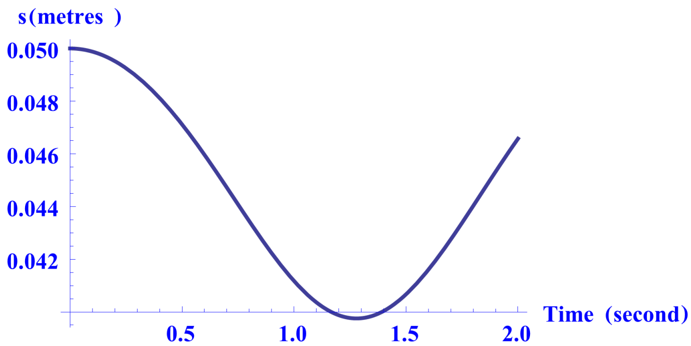

Figure 4.2: Variation of steering/rack input s with time.

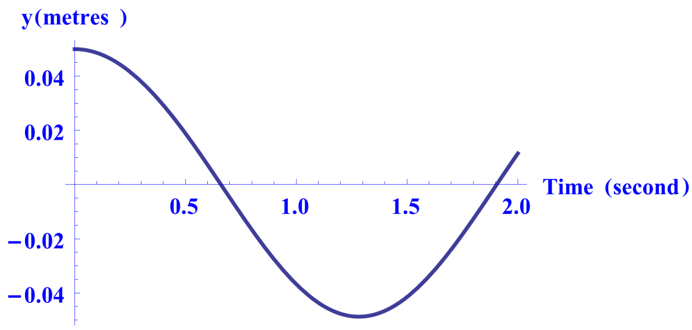

Figure 4.3: Variation of road profile input y with time.

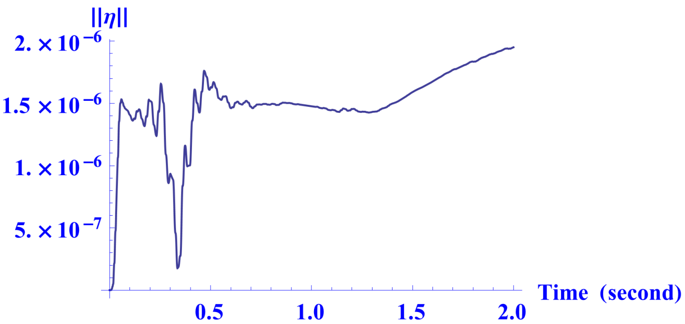

Figure 4.4: Variation of $||\eta||$ with time.

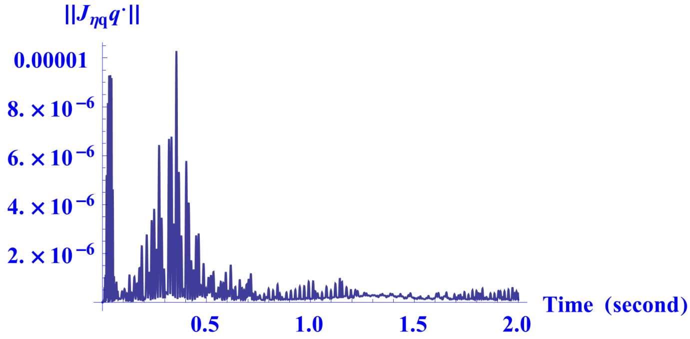

Figure 4.5: Variation of $\|\boldsymbol{J}_{\eta q}\dot{\boldsymbol{q}}\|$ with time.

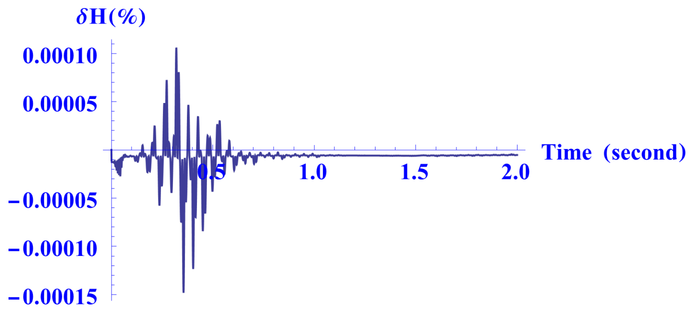

Figure 4.6: Percentage error in the conservation of total energy $\delta\mathbf{H}(\%)$ with time.

4.5.2 Results when spring and damper both are considered

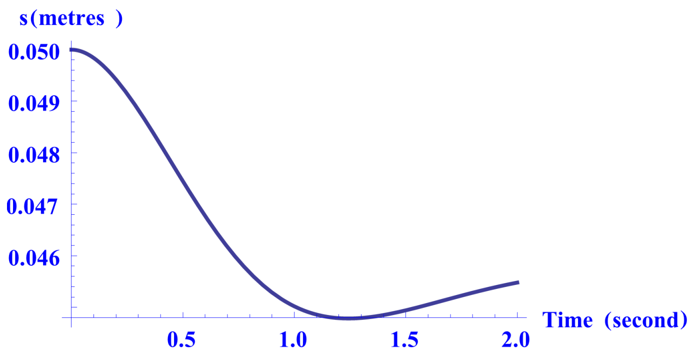

Figure 4.7: Variation of steering/rack input s with time.

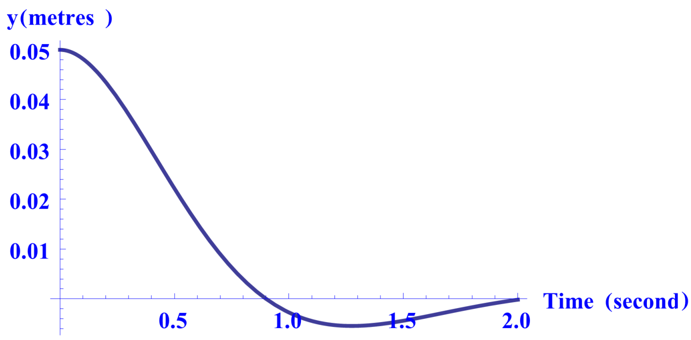

Figure 4.8: Variation of road profile input y with time.

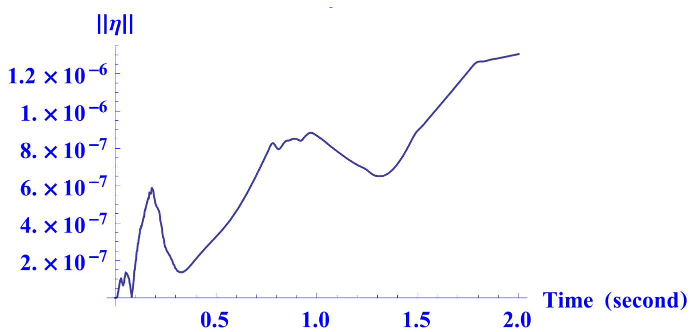

Figure 4.9: Variation of $||\boldsymbol{\eta}||$ with time.

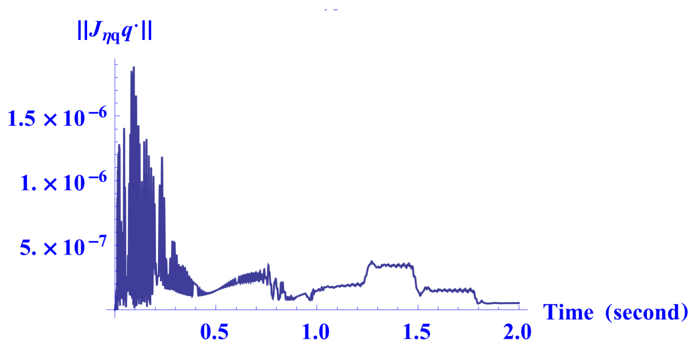

Figure 4.10: Variation of $\|\boldsymbol{J}_{\eta q}\dot{\boldsymbol{q}}\|$ with time.

4.6 Dynamic formulation in actuator space

The general equation of motion for rigid multi-body systems in actuator space can be written as:

$$\boldsymbol{M}_{\theta}\ddot{\boldsymbol{\theta}} + \boldsymbol{C}_{\theta}\dot{\boldsymbol{\theta}} + \boldsymbol{G}_{\theta} = \boldsymbol{\tau}_{\theta}, \tag{4.22}$$

Here, $\boldsymbol{\theta}$ represents the vector of active variables. The significance of the terms $\boldsymbol{M_\theta}$, $\boldsymbol{C_\theta}$ and $\boldsymbol{G_\theta}$ and their physical interpretation has been explained in the Chapter 2. The variables $\boldsymbol{\theta}=[s, y]^\top$ define the actuator space of the double wishbone suspension system, and are also termed as active variables. The variables which are dependent on $\boldsymbol{\theta}$ are termed as inactive variables, $\boldsymbol{\phi}=[\theta, \psi, l_8, c_1, c_2, c_3, x, z, \beta, \gamma, \delta_1, \delta_2]^\top$. Therefore, in DWB suspension system, there are 2 active variables and 12 inactive variables. Using the approach described in Chapter 2, one can get the actuator space from full configuration space. The advantage of actuator space is that the number of differential equations to solve the equation of motion of the system is reduced. For example, in DWB suspension system, the set of differential equation is reduced from 14 to 2 in actuator space, i.e., the system is reduced to a 2×2 system. The $\boldsymbol{M_\theta}$, $\boldsymbol{C_\theta}$ and $\boldsymbol{G_\theta}$ matrices are quite complex in nature compared to $\boldsymbol{M}, \boldsymbol{C}$ and $\boldsymbol{G}$. Since, $\boldsymbol{M_\theta}$, $\boldsymbol{C_\theta}$ and $\boldsymbol{G_\theta}$ will be dependent on inactive variables, therefore the forward kinematics has to be solved at every time step to solve the system of differential equations.

As mentioned previously, the formulation of the dynamics has been done in two parts:

1. Effect of spring has been included in the formulation of the dynamics.
2. Combined effect of spring and damper has been included in the formulation of the dynamics.

4.7 Method to solve equation of motion in actuator space

The double wishbone suspension system is reduced to a set of 2 simultaneous differential equations which is of the form as shown in Eq. (2.18). The set of 2 differential equations has to be solved in to understand the dynamics and behaviour of the system when applied with steering/rack input s and the road profile input y. It is computationally very expensive and very difficult to solve the differential equations analytically. Therefore, a numerical approach to solving differential equations has been implemented. The problem to solving differential equation has been approached in two manner and has been explained in detailed version along with their respective computational time.

4.7.1 Method 1

The set of differential equation is solved numerically by implementing a numerical integrator module using NDSolve in *Mathematica*. The flow chart in Fig. (3.13) describes the procedure. The simulation was conducted for t = 0 to t = 0.1 seconds with maximum number of steps 100 for the time interval. The computational time taken, i.e., CPU run time to obtain the solution was approximately 18.16 hours, which is computationally quite expensive. In this approach, the functions $f_1(c_1, c_2, c_3) = 0,\ f_2(c_1, c_2, c_3) = 0, f_3(c_1, c_2, c_3) = 0$, were evaluated using Solve command in *Mathematica*, which takes approximately 8.84 minutes for evaluation every time-step. Moreover, upon observation it was found that NDSolve command in *Mathematica* takes multiple steps to converge to a solution for a single time-step leading to higher computational time.

4.7.2 Method 2

The set of differential equations is evaluated by implementing a numerical integrator module and solving the set of equations using Runge-Kutta fourth order method. The flow chart in Fig. (3.14) describes the procedure. The simulation is performed for t = 0 to 2 seconds for step size of h = 0.001. An error of the order 10^{-5} is observed compared to the solution obtained from configuration space. The CPU run time taken to compute the solution was 2.38 seconds to compute the solution. In this approach, the functions $f_1(c_1, c_2, c_3) = 0,\ f_2(c_1, c_2, c_3) = 0, f_3(c_1, c_2, c_3) = 0$, were evaluated numerically using Runge-Kutta fourth order method at every time step.

In the Section 4.7, results obtained from method 2 have been presented along with the verifications that will validate the formulation of the DWB suspension system in configuration space.

4.8 Results of actuator space

4.8.1 Results when only spring is considered

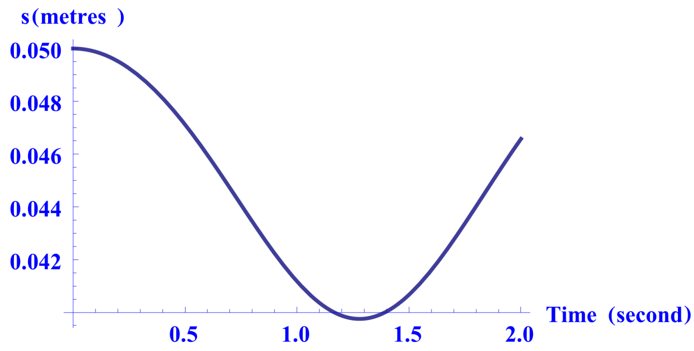

Figure 4.11: Variation of steering/rack input s with time.

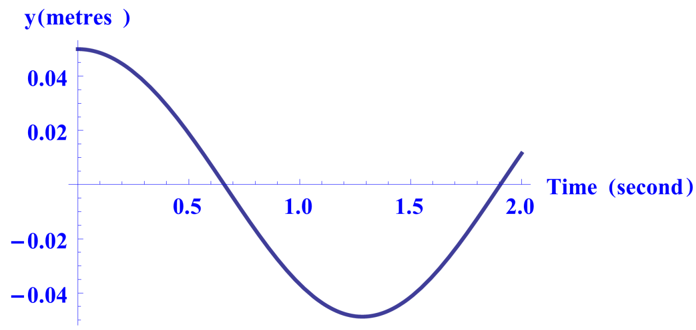

Figure 4.12: Variation of road profile input y with time.

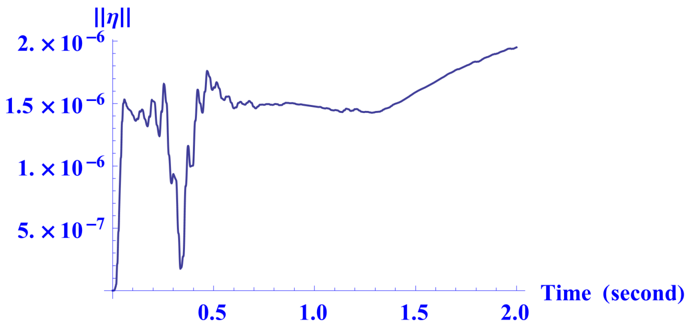

Figure 4.13: Variation of $||\eta||$ with time.

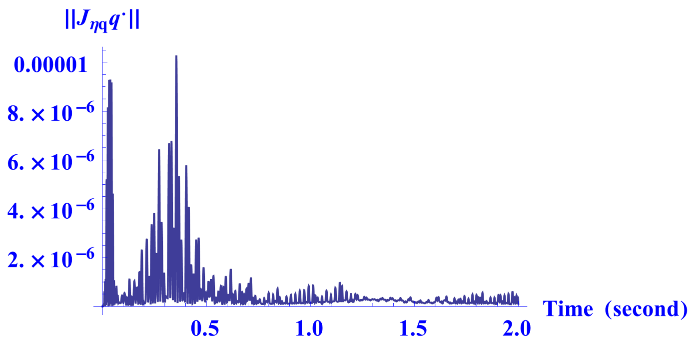

Figure 4.14: Variation of $\|\boldsymbol{J}_{\eta q}\dot{\boldsymbol{q}}\|$ with time.

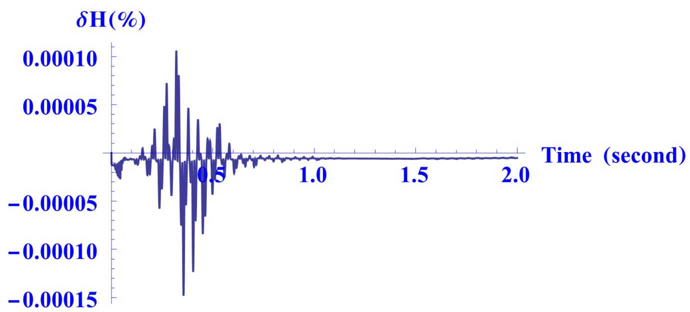

Figure 4.15: Percentage error in the conservation of total energy $\delta\mathbf{H}(\%)$ with time.

4.8.2 Results when spring and damper both are considered

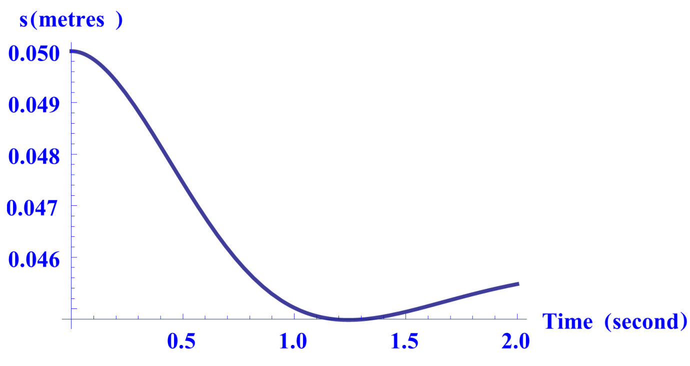

Figure 4.16: Variation of steering/rack input s with time.

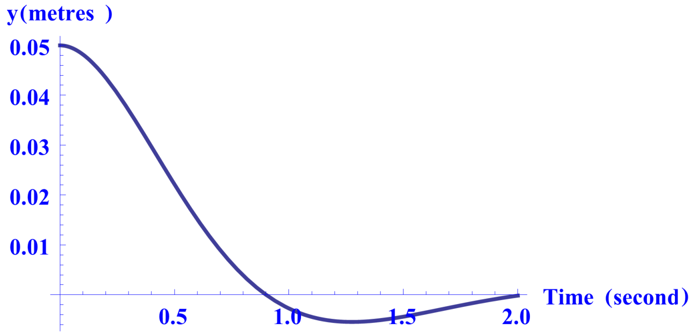

Figure 4.17: Variation of road profile input $\mathbf{y}$ with time.

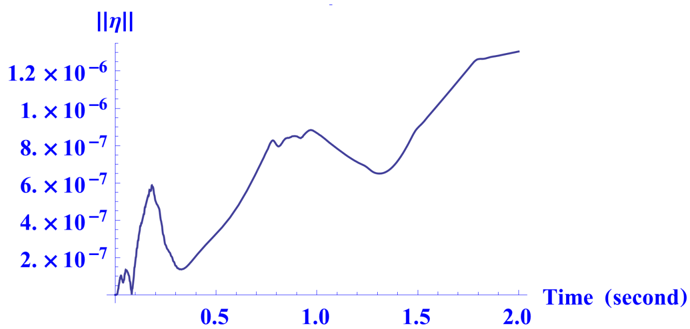

Figure 4.18: Variation of $||\boldsymbol{\eta}||$ with time.

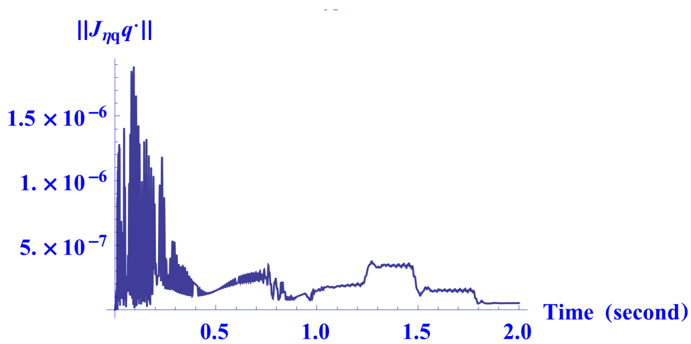

Figure 4.19: Variation of $||\boldsymbol{J}_{\eta q}\dot{\boldsymbol{q}}||$ with time.

CHAPTER 5

CONCLUSION AND FUTURE WORK

5.1 Overview

In this report, Lagrangian approach to formulate the dynamics of MPS and DWB is presented. Two different formulation has been proposed, one in configuration space and other in actuator space. Dynamics of MPS and DWB have been formulated using point formulation in various papers (see [4] and [5]). The advantage of Lagrangian approach over point formulation has been reported in the Table 5.1 with reference to the computational time taken to solve the system of dynamics equation of motion. Further, different methods to solve the system of equation of motion were proposed with their algorithm described in flowcharts. Below Table 5.1 and Table 5.2 describes the computational time of MPS and DWB suspension for actuator space and configuration space formulation while comparing with the dynamic model as proposed in [4] and [5].

Table 5.1: Computational time taken for MPS suspension for step-size, h = 0.001.

	Configuration space	Actuator space	Point-Formulation (in [5])
C.P.U run time (in seconds)	196.2	2.16	Not reported
Dimension of $\boldsymbol{M}$ matrix	11×11	2×2	Not reported

Table 5.2: Computational time taken for DWB suspension for step-size, h = 0.001.

	Configuration space	Actuator space	Point-Formulation (in [4])
C.P.U run time (in seconds)	376.2	2.34	5280
Dimension of $\boldsymbol{M}$ matrix	14×14	2×2	31×31

5.2 Future work

This work does not include the effect of vehicle dynamics on the steering and suspensions. And the simulations were performed for an arbitrary $\mathbf{s}$ and $\mathbf{y}$, without including the effect of driver controlled steering, which is required in case of maneuvers such as cornering, braking etc.

APPENDIX A

FORMULATION OF LOOP CLOSURE EQUATION

A.1 MacPherson strut suspension

There are two input to the suspension system, one being steering/rack input $\boldsymbol{s}$ acting at the point $\boldsymbol{p}_5$ and the other due to the road profile $\boldsymbol{y}$ acting at the point $\boldsymbol{p}_8$.

The end- points of the link 2 can be expressed as:

$$\boldsymbol{p}_1 = \boldsymbol{o}_1 + \boldsymbol{R}_Z(\theta)[l_1, 0, 0]^\top, \text{ and} \tag{A.1}$$

$$\boldsymbol{o}_2 = [o_{2x}, o_{2y}, o_{2z}]^\top, \tag{A.2}$$

respectively. The vector $\boldsymbol{l}_2$ can be expressed as:

$$\boldsymbol{l}_2 = \boldsymbol{o}_2 - \boldsymbol{p}_1, \text{ or} \tag{A.3}$$

$$\boldsymbol{l}_2 = {}^0_2\boldsymbol{R}[l_2, 0, 0]^\top. \tag{A.4}$$

From the Eq. (A.1)-(A.4), one can write:

$$\boldsymbol{o}_2 - \boldsymbol{o}_1 - \boldsymbol{R}_Z(\theta)[l_1, 0, 0]^\top - {}^0_2\boldsymbol{R}[l_2, 0, 0]^\top = \boldsymbol{0}. \tag{A.5}$$

Eq. (A.5) models the kinematics of the four-bar mechanism $\boldsymbol{o}_1\boldsymbol{p}_1\boldsymbol{o}_2\boldsymbol{o}_1$. The expression on the left hand side of Eq. (A.5) is of the form:

$$\boldsymbol{\eta}_1 = [\eta_{1x},\ \eta_{1y}, \eta_{1z}]^\top, \tag{A.6}$$

where η_{1x}, η_{1y} and η_{1z} are given by:

$$\eta_{1x} = - l_2\left(c_1^2 - c_2^2 - c_3^2 + 1\right) - c_\Delta l_1 \cos\theta + c_\Delta o_{2x}, \tag{A.7}$$

$$\eta_{1y} = - 2l_2(c_1c_2 + c_3) - c_\Delta l_1 \sin\theta + c_\Delta o_{2y}, \tag{A.8}$$

$$\eta_{1z} = - 2l_2(c_1c_3 - c_2) + c_\Delta o_{2z}, \tag{A.9}$$

$$\text{where, } c_\Delta = 1 + c_1^2 + c_2^2 + c_3^2. \tag{A.10}$$

The end points of link-5 can be expressed as:

$$\boldsymbol{p}_4 = \boldsymbol{p}_1 + {}^0_2\boldsymbol{R}[r,0,0]^\top + {}^0_2\boldsymbol{R}{}^2\boldsymbol{l}_4, \text{ and} \tag{A.11}$$

$$\boldsymbol{p}_5 = [p_{5x} + s_x, p_{5y} + s_y, p_{5z} + s_z]^\top, \tag{A.12}$$

where r is distance between $\boldsymbol{p}_1$ and $\boldsymbol{p}_3$; ${}^2\boldsymbol{l}_4$ is $[l_{4x}, l_{4y}, l_{4z}]^\top$(expressed in $\{2\}$) and $\boldsymbol{s} = [s_x, s_y, s_z]^\top$ is the rack input vector in $\{0\}$, given by:

$$\boldsymbol{s} = {}^3_0\boldsymbol{R}[s,0,0]^\top, \text{ where}$$
$${}^3_0\boldsymbol{R} = \boldsymbol{R}_X(\beta_1)\boldsymbol{R}_Y(\beta_2)\boldsymbol{R}_Z(\beta_3).$$

The vector $\boldsymbol{l}_5$ can be expressed as:

$$\boldsymbol{l}_5 = \boldsymbol{p}_5 - \boldsymbol{p}_4.$$

The loop-closure constraints of the five bar mechanism $\boldsymbol{o}_1\boldsymbol{p}_1\boldsymbol{p}_4\boldsymbol{p}_5\boldsymbol{o}_1$ can be reduced to the following equation:

$$\eta_2 = (\boldsymbol{p}_5 - \boldsymbol{p}_4)\cdot(\boldsymbol{p}_5 - \boldsymbol{p}_4) - l_5^2 = 0. \tag{A.13}$$

The expression on the left hand side of Eq. (A.13) is denoted by η_2. From the road input to the lower A-arm loop, $\boldsymbol{o}_1\boldsymbol{p}_1\boldsymbol{p}_6\boldsymbol{p}_8\boldsymbol{o}_1$, one can write:

$$[p_{8x} + x, p_{8y} + y, p_{8z} + z]^\top - {}^0_2\boldsymbol{R}{}^2\boldsymbol{l}_6 - {}^0_2\boldsymbol{R}[\rho,0,0]^\top - \boldsymbol{R}_z(\theta)[l_1,0,0]^\top - \boldsymbol{o}_1 = \boldsymbol{0}, \tag{A.14}$$

where x, z are variables, which vary upon changing s and y; ${}^2\boldsymbol{l}_6 = [l_{6x}, l_{6y}, l_{6z}]^\top$ is the vector from ${}^2\boldsymbol{p}_6$ to ${}^2\boldsymbol{p}_8$(expressed in $\{2\}$). The parameter ρ is the distance between $\boldsymbol{p}_1$ and $\boldsymbol{p}_6$. The expression on the left hand side of Eq. (A.14) is of the form:

$$\boldsymbol{\eta}_3 = [\eta_{3x},\ \eta_{3y}, \eta_{3z}]^\top. \tag{A.15}$$

where η_{3x}, η_{3y} and η_{3z} are given by:

$$\begin{aligned}
\eta_{3x} =& - l_{6x}\left(c_1^2 - c_2^2 - c_3^2 + 1\right) - 2l_{6y}(c_1c_2 - c_3) - 2l_{6z}(c_1c_3 + c_2) \\
& - \rho\left(c_1^2 - c_2^2 - c_3^2 + 1\right) - c_\Delta l_1 \cos\theta + c_\Delta p_{8x} + c_\Delta x, && \text{(A.16)} \\
\eta_{3y} =& - 2l_{6x}(c_1c_2 + c_3) - l_{6y}\left(-c_1^2 + c_2^2 - c_3^2 + 1\right) - 2l_{6z}(c_2c_3 - c_1) \\
& - 2\rho(c_1c_2 + c_3) - c_\Delta l_1 \sin\theta + c_\Delta p_{8y} + c_\Delta y, && \text{(A.17)} \\
\eta_{3z} =& - 2l_{6x}(c_1c_3 - c_2) - 2l_{6y}(c_1 + c_2c_3) - l_{6z}\left(-c_1^2 - c_2^2 + c_3^2 + 1\right) \\
& - 2\rho(c_1c_3 - c_2) + c_\Delta p_{8z} + c_\Delta z. && \text{(A.18)}
\end{aligned}$$

Using the elimination procedure as proposed in the Fig. A.1, three equations are evaluated $f_1(c_1, c_2, c_3) = 0$, $f_2(c_1, c_2, c_3) = 0$, $f_3(c_1, c_2, c_3) = 0$. The function f_i are quartic in nature and are used to extract the values of c_1, c_2, c_3 that will satisfy the functions obtained.

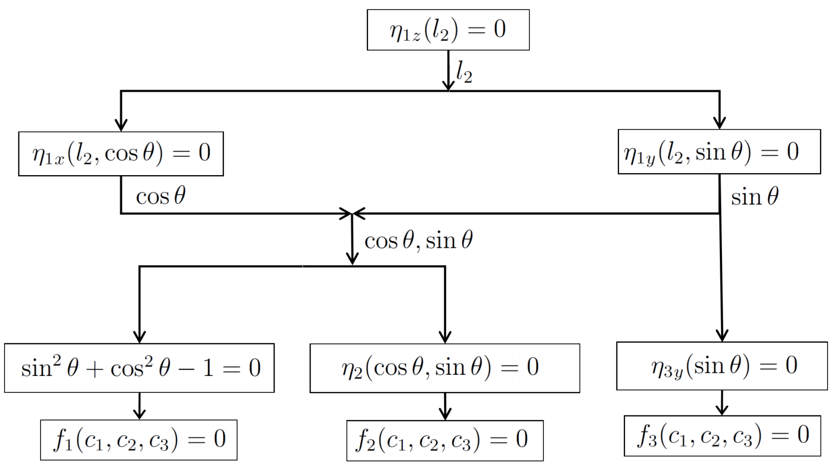

Figure A.1: Sequence of elimination of $\cos\theta$, $\sin\theta$ and l_2 (taken from [1]).

A.2 Double wishbone suspension

There are two input to the suspension system, one being steering/rack input ***s*** acting at the point p_5 and the other due to the road profile ***y*** acting at the point p_8.

The end points of link-2 can be expressed as:

$$\boldsymbol{p}_1 = \boldsymbol{o}_1 + \boldsymbol{R}_{Z_0}(\theta)[l_1, 0, 0]^\top, \text{ and} \tag{A.19}$$

$$\boldsymbol{p}_2 = \boldsymbol{o}_2 + {}^0_1\boldsymbol{R}\boldsymbol{R}_{Z_1}(\psi)[l_3, 0, 0]^\top, \tag{A.20}$$

respectively. The vector $\boldsymbol{l}_2$ can be expressed as:

$$\boldsymbol{l}_2 = \boldsymbol{p}_2 - \boldsymbol{p}_1, \text{ or} \tag{A.21}$$

$$\boldsymbol{l}_2 = {}^0_2\boldsymbol{R}[l_2, 0, 0]^\top. \tag{A.22}$$

From the Eqs. (A.19-A.22), one can write:

$$\boldsymbol{o}_2 - \boldsymbol{o}_1 + {}^0_1\boldsymbol{R}\boldsymbol{R}_{Z_1}(\psi)[l_3, 0, 0]^\top - \boldsymbol{R}_{Z_0}(\theta)[l_1, 0, 0]^\top - {}^0_2\boldsymbol{R}[l_2, 0, 0]^\top = \mathbf{0}. \tag{A.23}$$

Eq. (A.23) models the kinematics of the four-bar loop $\boldsymbol{o}_1\boldsymbol{p}_1\boldsymbol{p}_2\boldsymbol{o}_2\boldsymbol{o}_1$. The LHS of Eq. (A.23) is written compactly as:

$$\boldsymbol{\eta}_1 = [\eta_{1x},\ \eta_{1y}, \eta_{1z}]^\top, \tag{A.24}$$

where η_{1x}, η_{1y} and η_{1z} are given by:

$$\begin{aligned}\eta_{1x} =& - l_2\left(c_1^2 - c_2^2 - c_3^2 + 1\right) - c_\Delta l_1 \cos\theta + c_\Delta l_3 \cos\alpha_2(\cos\alpha_3 \cos\psi - \sin\alpha_3 \sin\psi) \\ & + c_\Delta o_{2x}, \qquad \text{(A.25)}\\ \eta_{1y} =& - 2l_2(c_1c_2 + c_3) + c_\Delta l_3(\cos\psi(\sin\alpha_1 \sin\alpha_2 \cos\alpha_3 + \cos\alpha_1 \sin\alpha_3) \\ & + \sin\psi(\cos\alpha_1 \cos\alpha_3 - \sin\alpha_1 \sin\alpha_2 \sin\alpha_3)) - c_\Delta l_1 \sin\theta + c_\Delta o_{2y}, \qquad \text{(A.26)}\\ \eta_{1z} =& - 2l_2(c_1c_3 - c_2) + c_\Delta l_3(\cos\psi(\sin\alpha_1 \sin\alpha_3 - \cos\alpha_1 \sin\alpha_2 \cos\alpha_3) \\ & + \sin\psi(\cos\alpha_1 \sin\alpha_2 \sin\alpha_3 + \sin\alpha_1 \cos\alpha_3)) + c_\Delta o_{2z}, \qquad \text{(A.27)}\end{aligned}$$

where, $c_\Delta = 1 + c_1^2 + c_2^2 + c_3^2$. (A.28)

The end points of link-5 can be expressed as:

$$\boldsymbol{p}_4 = \boldsymbol{p}_1 + {}^0_2\boldsymbol{R}[rl_2, 0, 0]^\top + {}^0_2\boldsymbol{R}{}^2\boldsymbol{l}_4, \text{ and} \qquad \text{(A.29)}$$

$$\boldsymbol{p}_5 = [p_{5x} + s_x, p_{5y} + s_y, p_{5z} + s_z]^\top, \qquad \text{(A.30)}$$

where rl_2 is distance between $\boldsymbol{p}_1$ and $\boldsymbol{p}_3$; ${}^2\boldsymbol{l}_4 = [l_{4x}, l_{4y}, l_{4z}]^\top$ (expressed in $\{2\}$), and $\boldsymbol{s} = [s_x, s_y, s_z]^\top$ is the rack input vector in $\{0\}$, given by:

$$\begin{aligned}\boldsymbol{s} =& {}^0_3\boldsymbol{R}[s, 0, 0]^\top, \text{ where} \\ {}^0_3\boldsymbol{R} =& \boldsymbol{R}_X(\beta_1)\boldsymbol{R}_Y(\beta_2)\boldsymbol{R}_Z(\beta_3),\end{aligned}$$

i.e., $(\beta_1, \beta_2, \beta_3)$ are XYZ Euler-angles relating the orientation of $\{3\}$ w.r.t.$\{0\}$. The vector $\boldsymbol{l}_5$ can be expressed as:

$$\boldsymbol{l}_5 = \boldsymbol{p}_5 - \boldsymbol{p}_4.$$

The closure equations of the five-bar loop $\boldsymbol{o}_1\boldsymbol{p}_1\boldsymbol{p}_4\boldsymbol{p}_5\boldsymbol{o}_1$ can be reduced to a single scalar equation:

$$\eta_2 = (\boldsymbol{p}_5 - \boldsymbol{p}_4) \cdot (\boldsymbol{p}_5 - \boldsymbol{p}_4) - l_5^2 = 0. \qquad \text{(A.31)}$$

The expression on the LHS of Eq. (A.31) is denoted by η_2. From the road input to the lower A-arm loop, $\boldsymbol{o}_1\boldsymbol{p}_1\boldsymbol{p}_6\boldsymbol{p}_8\boldsymbol{o}_1$, one can write:

$$[p_{8x}+x, p_{8y}+y, p_{8z}+z]^\top - {}^0_2\boldsymbol{R}^2\boldsymbol{l}_6 - {}^0_2\boldsymbol{R}[\rho l_2, 0, 0]^\top - \boldsymbol{R}_{Z_0}(\theta)[l_1, 0, 0]^\top - \boldsymbol{o}_1 = \mathbf{0}, \tag{A.32}$$

where x, z are the horizontal components of displacement of $\boldsymbol{p}_8$ w.r.t. $\{0\}$ as a consequence of s and y departing from their initial values; ${}^2\boldsymbol{l}_6 = [l_{6x}, l_{6y}, l_{6z}]^\top = {}^2\boldsymbol{p}_8 - {}^2\boldsymbol{p}_6$.

The parameter ρ is the fraction of distance between $\boldsymbol{p}_1$ and $\boldsymbol{p}_6$ of l_2 and is given by: $\rho = \|{}^0\boldsymbol{p}_6 - {}^0\boldsymbol{p}_1\|/l_2$. The expression on the LHS of Eq. (A.32) is of the form:

$$\boldsymbol{\eta}_3 = [\eta_{3x},\ \eta_{3y}, \eta_z]^\top, \tag{A.33}$$

where η_{3x}, η_{3y} and η_{3z} are given by:

$$\begin{aligned}
\eta_{3x} =& -l_2\rho\left(c_1^2 - c_2^2 - c_3^2 + 1\right) - l_{6x}\left(c_1^2 - c_2^2 - c_3^2 + 1\right) - 2l_{6y}(c_1c_2 - c_3) \\
& - 2l_{6z}(c_1c_3 + c_2) + c_\Delta\left(-l_1\cos\theta + p_{8x} + x\right), && \text{(A.34)} \\
\eta_{3y} =& -2l_2\rho(c_1c_2 + c_3) - 2l_{6x}(c_1c_2 + c_3) - l_{6y}\left(-c_1^2 + c_2^2 - c_3^2 + 1\right) \\
& - 2l_{6z}(c_2c_3 - c_1) + c_\Delta\left(-l_1\sin\theta + p_{8y} + y\right), && \text{(A.35)} \\
\eta_{3z} =& -2l_2\rho(c_1c_3 - c_2) - 2l_{6x}(c_1c_3 - c_2) - 2l_{6y}(c_1 + c_2c_3) \\
& - l_{6z}\left(-c_1^2 - c_2^2 + c_3^2 + 1\right) + c_\Delta\left(p_{8z} + z\right). && \text{(A.36)}
\end{aligned}$$

Using the elimination procedure as proposed in the Fig. A.2, three equations are evaluated $f_1(c_1, c_2, c_3) = 0$, $f_2(c_1, c_2, c_3) = 0$, $f_3(c_1, c_2, c_3) = 0$. The function f_i are quartic in nature and are used to extract the values of c_1, c_2, c_3 that will satisfy the functions obtained.

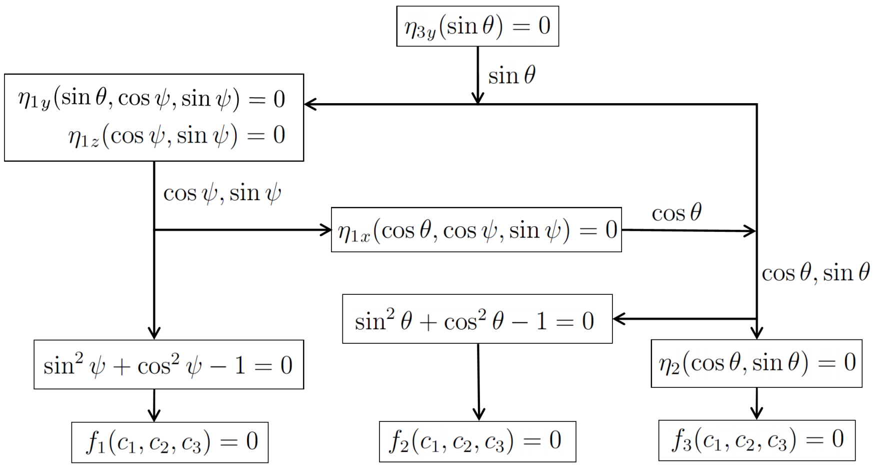

Figure A.2: Sequence of elimination of $\cos\theta$, $\sin\theta$, $\cos\psi$ *and* $\sin\psi$ (taken from [1]).

APPENDIX B

REFERENCES

[1] Kodati, Madhu, and Sandipan Bandyopadhyay. "Kinematic Analysis of the Double Wishbone Suspension System."

[2] T. D. Gillespie, Fundamentals of Vehicle Dynamics. Warrendale, PA: SAE International, 1992

[3] Ghosal, A., Robotics: Fundamental Concepts and Analysis. Oxford University Press, New Delhi, 2006

[4] H. A. Attia, "Dynamic modelling of the double wishbone motor-vehicle suspension system", European Journal of Mechanics A/Solids, vol. 21, pp 167-174, 2002.

[5] H. Attia, "Numerical kinematic analysis of the standard MacPherson motor-vehicle suspension system", KSME International Journal, vol. 17, no. 12, pp. 1961-1968, 2003.

[6] R. N. Jazar, Vehicle Dynamics: Theory and Application. Springer, 2008

[7] Press, William H., et al. "Numerical recipes, the art of scientific computing."American Journal of Physics 55.1 (1987): 90-91.

[8] Goldstein, H., C. P. Poole, and J. L. Safko, Classical Mechanics. Addison Wesley, 2001.